Studies of Novel Nanostructures by Cross- sectional Scanning Tunneling Microscopy

Ouattara, Lassana

2006

Studies of Novel Nanostructures by Cross-sectional Scanning Tunneling Microscopy

Lassana Ouattara

Department of Synchrotron Radiation Research
Lund University

THESIS FOR DEGREE OF DOCTOR OF PHILOSOPHY IN PHYSICS

Faculty Opponent:
Prof. Chris Palmström
Chemical Engineering and Material Science
University of Minnesota
Minneapolis, USA

LUND
UNIVERSITY

To be presented with the permission of the Faculty of Science of Lund University for public criticism in Lecture Hall B at the Department of Physics, December 1 2006, at 10:15.

Studies of Novel Nanostructures by Cross-sectional Scanning Tunneling Microscopy

Printed in Lund, Sweden, 2006, by Mediatryck

Department of Synchrotron Radiation Research
Institute of Physics
Lund University
Box 118
SE-221 00 LUND, SWEDEN

ISBN-10 91-628-6948-5
ISBN-13 978-91-628-6948-9
ISRN LUNDFD6/NFSF – 06/1030 – SE

Till: Sally Ouattara
Sara Otthén
Salimata Bamba

Abstract

This thesis presents structural and morphological studies of semiconductor nanostructures, namely quantum dots, nanowires and a dilute ferromagnetic semiconductor. These nanostructures are investigated on the atomic scale using cross-sectional scanning tunneling microscopy (XSTM).

Indium arsenide (InAs) quantum dots in both an indium phosphide (InP) and GaAs matrix are studied. The InAs/InP quantum dots are shown to be vertically aligned and I present experimental and theoretical investigations on the vertical correlation of the dots. The InAs/InP dots have a pure InAs stoichiometry, with intermixing occurring only at the outermost atomic rows, and they have a truncated pyramidal shape. In the case of InAs/GaAs quantum dots, their shape could best be approximated by an oval dot shape; they are intermixed contrarily to the InAs/InP dots and have a non-uniform size distribution. Furthermore, various defects are observed in the quantum dot structures and the surrounding material. The origins of these defects are discussed and compared to available theoretical predictions. One example of such defect is the spontaneous formation of an extra quantum dot in the grown structures. The spontaneously formed dot nucleates on top of the vertical stacks and is of the same nature as the seed dots. The formation of the extra quantum dot is attributed to phase segregation effects in the top GaInAs layer of the structure and As/P exchange reactions.

XSTM results on semiconductor nanowires are also presented. Using a special embedding scheme, individual atomic positions, stacking faults and different defects inside a GaAs nanowire are imaged. Moreover, I have investigated nanowire heterostructures, with wires containing an aluminium gallium arsenide (AlGaAs) segment and surrounded by an AlGaAs shell. It is shown that one of the interfaces between the wire and an embedded AlGaAs segment is sharp while the other one is diffuse and solutions on how to achieve sharp heterostructure interfaces and smooth shell capping are proposed.

Finally, the location sites of manganese (Mn) atoms in a Mn-doped gallium arsenide (GaAs) lattice are studied and the Mn atoms are found at gallium sites (substitutional Mn) in the second layer gallium. This knowledge is used to investigate the diffusion of Mn atoms in GaAs/GaMnAs superlattices and it is shown that approximately 20% of Mn is found to diffuse to the adjacent GaAs layers.

Keywords: *quantum dots, nanowires, dilute ferromagnetic semiconductors, superlattices, cross-sectional scanning tunneling microscopy, semiconductor nanostructures, epitaxy.*

Preface

”Lôni waliman saya, Nseko tè Abe Ndjori la.

The interpretation of the above sentence is left to your fantasy. Or read the thesis and find out!

The experimental work of this thesis was performed in the STM laboratories at the Department of Synchrotron Radiation Research, University of Lund, Sweden.

The thesis is based on structural and morphological studies of semiconductor nanostructures using cross-sectional scanning tunneling microscopy. A general summary of semiconductor physics and nanostructures is given, followed by a description of the experimental technique used. The results are summarized in chapter 4 and thoroughly presented in the enclosed papers.

Papers related to semiconductor quantum dots

I *Correlation lengths in stacked quantum dot systems: Experiment and Theory*
L. Ouattara, J. M. Ulloa, A. Mikkelsen, E. Lundgren, P. M. Koenraad, M. Borgström, L. Samuelson and W. Seifert.
Submitted to Nanotechnology.

II *A cross-sectional scanning tunneling microscopy study of a quantum dot infrared photo-detector structure*
L. Ouattara, L. Höglund, A. Mikkelsen, E. Lundgren, C. Asplund and J. Y. Andersson
J. Appl. Phys. **100**, 044320 (2006).

III *Stacked InAs quantum dots in InP studied by cross-sectional scanning tunneling microscopy*
L. Ouattara, A. Mikkelsen, E. Lundgren, M. Borgström, L. Samuelson and W. Seifert
Nanotechnology **15**, 1701 (2004).

IV *Spontaneous InAs quantum dot nucleation at strained InP/GaInAs interfaces*
M. Borgström, L. Samuelson, W. Seifert, A. Mikkelsen, L. Ouattara and E. Lundgren
Appl. Phys. Lett. **83**, 4830 (2003).

Papers related to semiconductor nanowires

V *Direct imaging of heterostructures inside a nanowire by scanning tunneling microscopy*
L. Ouattara, A. Mikkelsen, N. Sköld, J. Eriksson, T. Knaapen, E. Cavar, W. Seifert, L. Samuelson and E. Lundgren.
In manuscript.

VI *Nanowire growth and dopants studied by cross-sectional scanning tunneling microscopy*
A. Mikkelsen, N. Sköld, L. Ouattara and E. Lundgren
Nanotechnology **17**, S362 (2006).

VII *Direct imaging of the atomic structure inside a nanowire by scanning tunneling microscopy*
A. Mikkelsen, N. Sköld, L. Ouattara, M. Borgström, J. N. Andersen, L. Samuelson, W. Seifert and Edvin Lundgren
Nature Materials **3**, 519 (2004).

Papers related to dilute magnetic semiconductors

VIII *Mn diffusion in $Ga_{1-x}Mn_xAs$/GaAs superlattices*
A. Mikkelsen, L. Ouattara, H. Davidsson, E. Lundgren, J. Sadowski and O. Pacherova
Appl. Phys. Lett. **85**, 4660 (2004).

IX *Defect structure of $Ga_{1-x}Mn_xAs$: A cross-sectional scanning tunneling microscopy study*
A. Mikkelsen, B. Sanyal, J. Sadowski, L. Ouattara, J. Kanski, S. Mirbt, O. Eriksson and E. Lundgren
Phys. Rev. B. **70**, 085411 (2004).

Papers not included in the thesis

X *Quantum dots-in-a-well infrared photodetectors for long wavelength infrared detection*
L. Höglund, P. O. Holtz, L. Ouattara, C. Asplund, Q. Wang, S. Almqvist, E. Petrini, H. Malm, J. Borglind, S. Smuk, A. Mikkelsen, E. Lundgren, H. Pettersson and J. Y. Andersson
SPIE proceedings, Security and Defence, 11-14 sept 2006.

XI *Zkoumani polovodicovych heterostruktur metodou XSTM*
O. Pacherova, E. Lundgren, A. Mikkelsen, L. Ouattara and H. Davidsson
Czech. J. Phys. A**56**, 90 (2006).

XII *Co on Mo(110) studied by scanning tunneling microscopy*
A. Mikkelsen, L. Ouattara and E. Lundgren
Surf. Sci. **557**, 109 (2004).

Comments on my own contribution to the papers

In all of the papers listed above I have done all or part of the measurements. For the papers where I am the first author I have, in addition to being responsible for the measurements, done the analysis of the data as well as written the paper. For the papers where I am not the first author my contribution is reflected by the position in the author list.

Acknowledgements

I would like to address my gratitude to my supervisors Docent Edvin Lundgren and Docent Anders Mikkelsen for all help and guidance throughout this thesis. I lack of enough adjectives to describe the support you provided me. Many thanks to you and your respective families.

I am further indebted to Prof. Koung-An Chao and Prof. Jesper Andersen for encouraging me for Ph.D studies. Koung-An and Jesper, thank you for considering me as a potential Doctor in physics and for believing in me.

No sample, no STM, no STM, no thesis, right? Therefore, many thanks to Prof. Lars Samuelson, Prof. Werner Seifert, Niklas Sköld, and Dr. Magnus Borgström for all the nice samples and a wonderful collaboration, and especial thanks to Niklas for fruitful discussions.

This thesis is also the result of very nice collaborations with different institutions as well as a company. I therefore address my gratitude to the people at the Technical University of Eindhoven, The Netherlands, namely Dr. Jose Maria Ulloa and Prof. Paul Koeenrad; to Dr. Oliva Pacherova at the Institute of Physics, Faculty of Mechanical Engineering, Czech Republic, and to Acreo ABs people, Linda Höglund, Dr. Carl Asplund and Prof. Jan Andersson. Linda, thanks for your friendship and fruitful discussions; It is a pity that our collaboration started so late.

A number of people has made my living and daily work easier and joyful. Thanks to - Werner Hofer (Liverpool), Lotta, Stacey, Ingolf, Joakim (thanks for your great comments), Andrea, Rasmus, Suomi, Emeli, Christina, Struan, Mikael Johansson, Henrik, Thijs, Åsa Magnusson, Martin Andersson, Annika, Hanno, Anti. Especial thanks to Elizabeta Cavar, Jessica Eriksson, Andreas Lindgren, Johan Gustafson and Micke Borg for what you have done for me. Then, my friends outside academia, the list is too long but you know that you mean a lot to me: Koffi, Alain, Noche, Madou Berthé... merci les gos et gars! Ya fohi!. To my friends Åsa, Lina, and Michel I say puss och kram. Marcus, Ludde, Hampus, I am glad that you guys exist! Jessica Nilsson, Carro, Sabina Gasic, Pia... thank you. Many thanks also to Max Souma, Eva, Soriba Touré (Tès) and Sal Dibba, the djembe has inspired me a lot! Thanks to The Otthéns, The Otthéns and The Lavessons for all support.

To my family in Ivory-Coast you inspire me everyday. I love you. Finally, I am extremely grateful to my girlfriend Sara Otthén and my daughter Sally Ouattara, for continuous support and for always being there for me. Madou/Adja, there is a meaning that you decided to come at the right time! This thesis is for you too. I save you guys for the end because you are the very best. I love you!

Peace and Love!!! /Lasso

Contents

Chapter 1

Introduction

Microelectronics have an evident strong impact on our daily life. Ipod nanos, cellular phones, compact disc players, childrens toy, not to mention computers are some examples. The pillar of these devices is the semiconductor technology or silicon technology. With the increasing need to fabricate more reliable, extremely fast and more powerful devices at very low costs by for example increasing the packing density and the data processing rates of integrated circuits, in order to satisfy the demands on new technologies and device functionalities, a miniaturization of devices and device components becomes a constraint. We have thus to rely on nanoelectronics, nanooptics, and nanosystems to replace or complement the limitations of the established silicon technology in the nearest future. The building stones for the nanodevices or quantum devices is III-V semiconductor nanostructures (1-100 nm) like quantum wells, nanowires and quantum dots, which have, due to their reduced dimensions, a high degree of electron confinement, which induces energy quantization effects (see chapter 2.2).

In order to provide materials and structures that can cope with the technology demands of nanodevices, embedded nanostructures in III-V semiconductors have been studied intensely for at least two decades. Due to the wide variety of III-V materials combinations and doping possibilities, the prospect of future nanostructures for novel and improved applications is very bright. Nanosystems present in fact fascinating results giving rise to challenges of well established areas in solid state physics research. However, controlling the fabrication processes and the characteristics of nanostructure-based devices requires a complete understanding of the structures on the atomic scale. The positions of single atoms inside a structure or at the interface between the structure and the surrounding material may significantly affect the properties of the material. Consequently, atomic-scale studies of such structures are extremely valuable. A unique and outstanding powerful technique to explore the atomic-scale arrangement of buried structures inside III-V semiconductors is cross-sectional scanning tunneling microscopy (XSTM). Thus, a number of reviews has been written on the topic [1-4].

In this thesis, XSTM is used to investigate buried III-V semiconductor nanostructures on the atomic scale: ferromagnetic (GaAs/GaMnAs) superlattices, InAs quantum dots (QDs) in both InP and GaAs and free-standing GaAs nanowires. Substantial knowledge that is necessary to understand the properties and characteristics of theses structures is provided. The InAs quantum dots in InP are vertically aligned, and are composed of pure InAs. Different defect structures as the spontaneous growth of extra quantum dots or defects such as the formation of semiconductor rings to give some examples are presented. It is shown by investigating

the spacer layer dependence of the stacked QDs how to improve the growth parameters of stacked QDs in order to control their size and vertical alignment. The thesis presents important results on a quantum dot infrared photodetector structure in which the QDs have an InGaAs stoichiometry. The results on the composition and size distribution of these QDs can be used to trace the emission wavelength of the photodetector. Furthermore, the results on the precise sites of Mn atoms in a GaMnAs film and the diffusivity of Mn atoms in a GaAs/GaMnAs superlattice contribute to an enhanced knowledge about the defects in these structures, how to control the growth of GaAs/GaMnAs superlattices and to understand the ferromagnetic behavior of such structures.

Finally, I report the first and unique XSTM results on free-standing GaAs nanowires. Using a special developed embedding scheme, individual atomic positions, stacking faults and different defect structures inside a nanowire are imaged. (My impression is that, our XSTM results on nanowires have contributed to the world-leading position in nanowire research of the nanometer structure consortium at Lund University).

The thesis is organized as follow: an introduction to semiconductor physics, nanostructures and epitaxy is first given. Then, the experimental technique used to explore these nanostructures on the atomic level is described. The enclosed papers constituting the framework of the thesis are summarized in chapter 4.

My hope is to contribute to an enhancement of our knowledge in nanoscience and nanotechnology through this thesis . A targeted audience is a Ph.D. student who has just initiated studies in nanophysics as well as non-experts in the field or anyone interested in nanophysics and/or cross-sectional scanning tunneling microscopy.

Chapter 2

Semiconductor materials and growth

This chapter presents an introduction to crystalline materials, semiconductors in general, and dilute ferromagnetic semiconductors. Some low-dimensional structures and their potential applications are presented. Furthermore epitaxy, oriented crystal growth on an underlying substrate, is briefly discussed. For more detailed reading see references [5-7].

2.1 Crystalline materials and semiconductors

A crystalline material is a regular array of atoms or ions. An ideal crystal is thus made of an infinite repetition of identical structural units in space. In the simplest crystals the structural unit is a single atom, but the smallest structural unit cell may be composed of many atoms or molecules. All crystal structures can be described in terms of a lattice with a group of atoms, the basis, attached to every lattice point. Material properties such as thermal, optical, and electrical properties will be dependent of the specific crystalline structure. Considering the electrical properties in terms of electrical conductivity, crystalline materials can be classified in three different groups: metals or conductors, semiconductors and insulators.

In single atoms, electrons reside in discrete energy states or levels. When an assembly of atoms are joined to form a crystal, the valence electrons originally bound to the attractive potential of one nucleus now interact with the potential of other nuclei. Consequently, the energy levels of individual atoms are rearranged in order to minimize the total energy of the system. This rearrangement results in the formation of extremely closely spaced levels that can be considered as a continuous band of energy in the solid state. One refers to these bands as valence band and conduction band. Between the energy bands there exist regions of forbidden states called bandgaps.

Depending on the electronic configuration of each atom and the separation between the atoms in the crystal the band structure will be characteristic for the crystal. In other words the band structure will define the electronic and optical properties of the crystal. The localization of the Fermi level, the highest occupied energy state, and the band filling will in fact characterize the material: metal, semiconductor, or insulator. The population of the

available states is given by the Fermi-Dirac distribution function:

$$f(E,T) = \frac{1}{1 + e^{\frac{(E-E_F)}{k_B T}}} , \tag{2.1}$$

where E_F is the Fermi energy and k_B is Boltzmann constant. The Fermi-Dirac distribution function gives the probability of finding an electron in a state of energy E at a given temperature T.

A metal is characterized by a very low electrical resistivity. The valence band is not entirely filled and the Fermi level lies in the valence band. Empty electronic states are thus available for carrier transport and electrons can very easily participate in current conduction when an electric field is applied. Metals are therefore good electric conductors.

In an insulator there is a large energy gap (5-10eV) between the highest occupied electronic state in the pure crystal and the lowest unoccupied one. All energy states in the valence band are occupied and all states in the conduction band are empty. Furthermore, the electrons form strong bonds between neighboring atoms even at room temperature. There are thus no free electrons to generate a current.

Semiconductors are materials which have intermediate conductivity properties between those of metals and insulators due to their special arrangement of the electronic energy levels [5, 6, 7]. They have a similar band structure to insulators, but with a much smaller energy gap (0.5-2eV). Because of the small bandgap, electrons in the valence band can be thermally excited to the conduction band. Since there are many empty states in the conduction band, a small applied potential can easily move these electrons and generate a current. The conductivity of a semiconductor can be increased by doping the semiconductor material. When impurity atoms are introduced into the material the semiconductor material is said to be doped. Impurity energy levels are introduced in the bandgap. Depending on the nature of the impurity atom, the Fermi level will move closer to the valence band (p-type doping) or closer to the conduction band (n-type doping).

Semiconductors are generally classified into four groups: the pure group IV elements like Si and Ge, the III-V compounds (GaAs, InAs, InP), which are combinations of group III and group V elements, the II-VI (ZnS, CdS), and IV-IV (SiC, SiGe), compounds. III-Vs are direct bandgap semiconductors meaning that electronic transitions from valence to conduction band occur without change of momentum. III-Vs are therefore suitable and attractive for optical device applications. The interesting optoelectronic properties of the III-Vs is one of the reasons which make them extensively used and studied.

2.2 Low-dimensional structures

Solids have optical and electronic structures which depend on the chemical nature of their atoms and the crystalline structure the atoms are arranged in. Bulk crystals have continuous energy band states, separated by gaps (bandgap) of forbidden energy levels as mentioned in the previous section. In order to tailor a crystal for a desired electronic or optical property a technique called bandgap engineering can be used. By using epitaxial techniques one can for example combine two or more semiconductors with different bandgaps and create a so-called heterostructure. Fig. 2.1 illustrates a heterostructure band-offset where a smaller bandgap semiconductor A is combined with a larger gap semiconductor B. A consequence of the

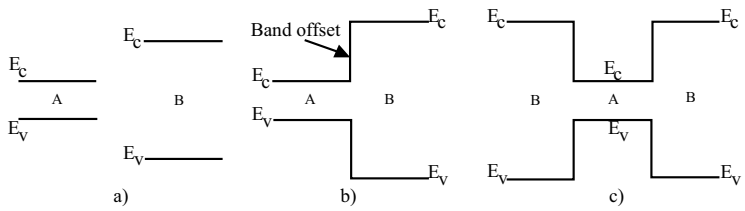

Figure 2.1: Schematic illustration of a heterostructure band offset, where a smaller bandgap semiconductor A is combined with a larger gap semiconductor B, a) A and B separated, b) the band offset structure after combination of A and B, c) a quantum well structure. E_C = conduction band edge, E_V = valence band edge.

resulting structure (Fig. 2.1b) is that an electron in material A is unable to overcome the energy barrier and enter into semiconductor B. The band offset becomes a potential barrier. Furthermore, an electron "living" in the conduction band of material B can lower its energy by jumping across the heterointerface to the conduction band of material A. Hence electrons can be confined to one side of the barrier.

In this way an interesting structure can be made by constructing a structure of type BAB (Fig. 2.1c), in which electrons (and/or holes) can be confined. It is a standard quantum mechanical particle in a box structure. If the sandwiched low bandgap material is a very thin film, one obtains a quantum well structure, which is a low-dimensional structure with extensions in one direction comparable to the de Broglie wavelength of electrons. In such a thin film, the motion of the carriers is restricted to two dimensions. By shaping the sandwiched material (A) into a very narrow wire into which the charge carriers are confined, one gets a one dimensional quantum wire. Extensively studied quantum wires are carbon nanotubes and semiconductor nanowires (whiskers) which have a broad range of possible applications (see section 2.2.3). A zero dimensional structure called quantum dot or quantum box is obtained by a further reduction of the dimensions of a quantum wire. The charge carriers are then confined in a very small volume of material A. Quantum dots possess interesting optoelectronic properties and have a large range of potential applications (see section 2.2.2). Fig. 2.2 shows the density of states of the electrons in connection to the dimensionality of the

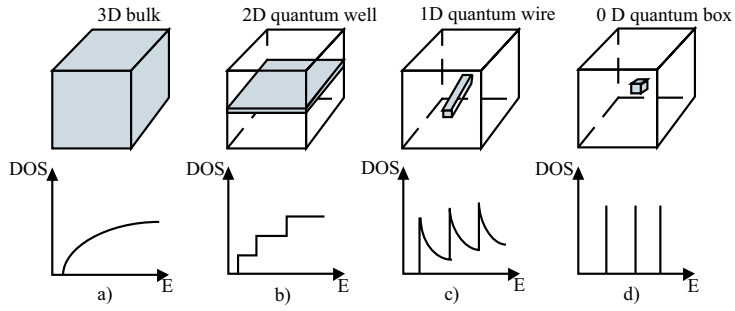

Figure 2.2: Density of state (DOS) as a function of energy state and dimensionality of the crystal, a) 3D, b) 2D, c) 1D and d) 0D structure.

crystals.

2.2.1 GaMnAs/GaAs superlattices

Dilute ferromagnetic semiconductors like GaMnAs are materials that exhibit both semiconducting and ferromagnetic properties. Since the charge of an electron provides the possibility to process information and its spin the realization of magnetic information in data storage devices, the usage of both properties within the same material is highly desirable.

Semiconductor materials like gallium arsenide (GaAs) or indium arsenide (InAs) can be doped by for example manganese (Mn) atoms to form a dilute ferromagnetic semiconductor material. The ferromagnetism and other properties of the material will depend on the concentration and precise site of the Mn atoms in the GaAs or InAs lattice. GaMnAs becomes ferromagnetic for more than 1-2% of Mn positioned at Ga sites [4, 8]. In such materials both local moments and holes are provided by the Mn atoms replacing Ga atoms. Mn acts both as an acceptor and source of local moments inducing the desired ordered state for ferromagnetism.

The intense research on Mn-doped III-V semiconductors initiated in the late 1970s [9, 10, 11], followed by the discovery of ferromagnetism in $Ga_{1-x}Mn_xAs$ by Ohno et al., 1996, [12] has been focused on the following frontlines: the fundamental physics that occurs in these systems and the material research aspect in order to increase the critical Curie temperature (T_c) for applications in so-called spintronic devices with novel spin based functionalities.

In Mn-doped III-V ferromagnetic semiconductors the material quality and magnetic properties are closely related, motivating the research performed on GaMnAs in this thesis. The potential applicability of ferromagnetic semiconductors in microelectronic technologies requires increased Curie temperatures from the current record of 173 K in GaMnAs epilayers to beyond room temperature [8, 11]. Theoretical calculations have shown that a T_c of 300 K or above could be achieved for Mn concentrations around 10% [13]. However, introducing such large amounts of Mn into the GaAs lattice induces considerable strain in the lattice. At high growth temperatures (higher than 520 K) MnAs precipitates are formed in the GaAs lattice, which is undesirable. Consequently, the growth temperature has to be kept below 520 K to avoid this situation. It has also been shown that these low temperatures are necessary for the Mn atoms to occupy the Ga sites [14]. Hence, there exist inherent difficulties to grow GaMnAs with 10% Mn content in Ga sites. Further, carrier density measurements have indicated that unwanted carrier-compensating defects are present in the structures. It has also been found that an increased Mn content in Ga sites increases the number of defects in the grown material. Compensating defects such as As anti-sites and Mn interstitial have thus been reported. However, the formation process of defects complexes is still not well-understood. Since some of these defects have been found to be energetically metastable, post-growth annealing methods have been used in order to modify important parameters such as the lattice constant, the hole density and the ferromagnetic transition temperature [8, 15]. The post-growth annealing process increases the Curie temperature by reducing the population of Mn interstitials [8]. Whether or not it will be possible to reach T_c above room temperature for Mn-doped III-V dilute ferromagnetic semiconductors is still an open question.

A GaMnAs/GaAs superlattice is a low-dimensional dilute ferromagnetic semiconductor

structure made of alternating layers of GaMnAs and GaAs repeated a certain number of times. Depending on the concentration of Mn in the GaMnAs layers, one will thus obtain a structure with alternating layers of a ferromagnetic GaMnAs material and non-magnetic GaAs material. An electronic device based on such a structure would include both non-magnetic device properties and spin-based magnetic device properties. The structures studied in this thesis consist of a superlattice structure with 32 monolayer $Ga_{1-x}Mn_xAs$ and 60 monolayer GaAs spacers, repeated 10 times. Different samples containing 1% and 5% of Mn were grown. A short period superlattice was also grown, consisting of 8 monolayer $Ga_{1-x}Mn_xAs$ and 4 monolayer of GaAs, with x = 0.05. The main purpose of this study was to investigate the diffusion of Mn from the GaMnAs layers to the adjacent GaAs.

I have also studied thick film samples composed of 1 micron GaMnAs films capped with 1 micron GaAs in order to investigate the Mn sites in the GaMnAs film. Before the growth of the GaMnAs films, a short period AlAs/GaAs superlattice was grown in order to easily localize the GaMnAs layers in the sample. The structure was covered with 0.5 mm low temperature grown GaAs. The samples in both studies were grown by Molecular Beam Epitaxy (MBE).

Potential applications

GaMnAs/GaAs superlattices are expected to be used for so-called spintronic devices [8, 12, 16], where the spin of electrons (or their resulting magnetism) is used to achieve novel and improved device functionalities. These novel devices and device functionalities are for example spin transistors, memories, higher speed, and lower power tunable detectors and lasers, and Q-bits for quantum computing.

2.2.2 Quantum dots (QDs)

Quantum dots are nanometer-size structures in which electrons are confined in all three dimensions. They have interesting features due to the high degree of quantization induced by the almost zero-dimensional degree of freedom for the electrons. Like an atom, quantum dots have discrete electronic energy levels as was shown in Fig. 2.2d and can therefore be considered as artificial atoms. However, the analogy between atoms and quantum dots is limited. A quantum dot can contain 10^4 atoms or more and the emission linewidths for example are often not limited by radiative lifetime, but are also affected by interactions with fluctuating charges in the dot surroundings and by interactions with the crystal lattice [17] containing the QD. Quantum dots can be made using lithographic and etching techniques [18, 19]. However, one of the most frequently used method today is a Stranski-Krastanow based self-assembly method (see also the section on epitaxy). Such an *in-situ* epitaxial method produces coherent, defect and dislocation free quantum dots. Coherent quantum dots are important for many application purposes.

Nanometer-size semiconductor inclusions in glass (Rocksby, 1932) which have been commercially available as color filters for decades were the first realization of quantum dots. These quantum dots are however not useful for electronic and optoelectronic devices because of the isolating matrix hindering electric injection. The dots studied in this thesis are Stranski-Krastanow self-assembled dots and their growth method will be described in more detail in section 2.3.

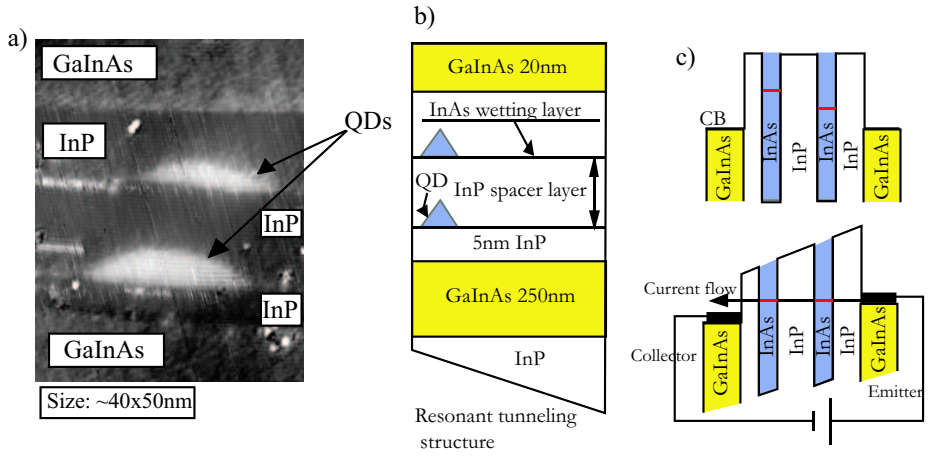

Figure 2.3: a) STM image of a stack of two QDs, b) schematic illustration of the model structure, c) model of a resonant tunneling device.

Applications

Quantum dots have a number of electronic and optical applications. They can be used in a resonant tunneling device structure as demonstrated in refs [20, 21, 22]. Quantum dots are also used as the active medium in lasers since they have good temperature stability, and low threshold current and emit light with a narrow linewidth [23]. Several groups [24, 25, 26] have demonstrated that quantum dots can be used in laser structures and quantum dot based lasers are commercially available [27]. Because of the emission wavelength found at a value close to 1.55 μm as for example in InAs/InP quantum dots as studied in this thesis, they are suitable for optical communication [24]. Quantum dots have also a potential application in quantum cryptography [28] since a single QD can be tuned to emit a single photon on demand [29, 30]. Furthermore, quantum dots are suitable for high density memory devices that can write and read information [31].

Stacked quantum dots for resonant tunneling devices or laser structures

Vertically stacked columns of quantum dots have been known to exist for more than 10 years [32, 33]. To achieve vertical alignment of the quantum dots a wetting layer with subsequent Stranski-Krastanow seed dots is grown. The dots in the following grown layers arrange themselves on top of the seed dot and of each other if the separating material between them is not too large, due to a strain field induced by the lower lying dots.

One of the projects of my PhD thesis was the structural investigation of vertically stacked InAs quantum dots, a structure for which resonant tunneling has been demonstrated [20, 21, 22]. Vertically stacked QDs are also used as an active medium for the fabrication of lasers [24, 25, 26]. The dots are shown to be well-correlated vertically, have a truncated pyramidal shape and a pure InAs stoichiometry.

Figs. 2.3a and b show an STM image of a stack of two InAs quantum dots in InP and a schematic illustration of the model structure. In Fig. 2.3c a schematic of the resonant

tunneling device is illustrated.

Resonant tunneling was first demonstrated by Chang et al. in 1974 [34]. In resonant tunneling the electrons in the emitter that have the same energy as the eigenstates localized between the barriers have an increased tunneling probability. At zero applied bias voltage no current will flow through the structure since the barrier is too large, unless the thermal energy is large enough so that the electrons can jump over the barrier. For a specific applied voltage the Fermi level of the emitter will align with the energy level in the dot. Due to the wave nature of the electrons one now has a finite probability for the electrons to tunnel to available states in the collector. As a consequence a current flow through the structure. This phenomenon is called resonant tunneling.

InAs/InGaAs/GaAs QDs for infrared-photodetector applications

Quantum dot based infrared photo-detectors (QDIPs) could have important applications on our daily life since QDIPs can be used in night vision camera detection systems for security and defence purposes. They can also be used for remote sensing and for chemical spectroscopy [35]. A recent and advanced technique for reaching the long wave infrared (LWIR) region is by embedding the InAs QD in an $In_xGa_{1-x}As$ quantum well, a so called DWELL structure, where the detection wavelength is partly determined by the surrounding quantum well [36, 37]. This approach offers new opportunities in tuning the detection wavelength to the region of interest. By adjusting the width and composition of the quantum well the energy level of the final state of the intraband transition can be shifted, which results in a shift of the detection wavelength [38, 39]. For infrared photo-detector applications DWELL-QDIPs are advantageous compared to conventional quantum well infrared photo-detectors since the use of QDIPs yields lower dark currents and higher photoelectric gains [35, 40, 41]. However, there still remain some major challenges for achieving full functionality of QD based photo-detectors. It has for example been difficult to accurately predict their operating wavelength, since the energy levels involved in the intrasubband transitions relevant for such detectors are dependent on the shape, size, and composition of the QDs [40]. For instance, the influence of the QD on the width of the quantum well due to intermixing may have a major influence on the detection wavelength. Knowledge of the level of intermixing between the QD and the quantum well is important when designing the QDIP for a certain detection wavelength. Thus, detailed information on these structural issues of buried sample structures are highly relevant. Therefore, I have studied a QDIP structure on the atomic level and provide substantial information for the realization of such structures. Detailed information on the growth of the QDIP structure and the experimental results are presented in paper II.

2.2.3 Nanowires

Nanowires, or whiskers as they are sometimes called, are one-dimensional rod-like structures in which carriers are confined in two dimensions to a few nanometers or tens of nanometers. Research on micron-thick whiskers was already active in the 1960s with the pioneering work of Wagner and Ellis [55]. It was, however, in the early 1990s that a method for nanowire growth with dimensions on the nanometer scale (10-100 nm) was developed by Kenji Hiruma [43] at Hitachi Central Research Laboratory in Japan, initiating thereby nanowire growth based on epitaxial techniques.

Nanowires can be synthesized using a top-down or bottom-up fabrication method. In the top-down approach as pioneered by Randall and Reed [19] at Texas instruments in the late 1980s, advanced lithographic tools were used to design a wire from a quantum well structure by for example Ohmic lift-off and anisotropic etching. However, this approach is rather unsatisfactory in relation to some applications because of fabrication damages. The method also suffers from a poor lateral control of the process. In the bottom-up method as initiated by Hiruma et al. [43], free standing nanowires are grown from a substrate surface, seeded by metal particles such as gold using epitaxial techniques. As a result, nanowires can be grown with a high crystalline quality and which are suitable for optical and optoelectronic applications in a controlled way. A large research effort has recently been devoted to nanowires because of their potential application in for example future electronic devices, in medicine, and biology.

Potential applications

As mentioned above the reason for the intense research on nanowires in recent years is their potential applicability in future electronic and photonic devices [44, 45]. The III-V nanowires provide a great possibility to create complex confined structures with a high degree of flexibility. For instance, heterostructures as well as well-defined correlated quantum dots can be grown inside the nanowire. Further, co-axial core–shell wires and even nanowires with their surfaces coated for particular sensor applications can be grown. Novel nanowire based devices like field effect transistors (FETs) [46], photodetectors [47], and single electron memories [48] have already been realized in the laboratory [49, 50]. Nanowires have also a great application potential in biology and medicine. The increased surface to volume ratio of nanowires can affect their sensitivity to chemical or biochemical substances. Cui et al. have presented the use of nanowire to measure pH [51] or to detect different types of cancer [44]. However, the need of a high degree of control of for example the nanowire growth is still a major challenge. To facilitate the control of nanowire growth processes significant improvements in our understanding of nanowire growth is necessary. Hence, methods that can directly probe the interior of the wire structure on the atomic scale are extremely important. Cross-sectional scanning tunneling microscopy (XSTM) is such a method as demonstrated in this thesis (see papers related to the characterization of nanowires).

2.3 Epitaxy

The nanostructures investigated in this thesis have been grown using different epitaxial techniques. The quantum dots and nanowires were grown by self-assembly processes using metalorganic vapor phase epitaxy (MOVPE). The ferromagnetic structures were grown using molecular beam epitaxy (MBE). Therefore, an overview of epitaxy and different growth modes is presented below.

2.3.1 Crystal growth

Epitaxy is an oriented crystal growth process used to grow high-quality, defect-free single-crystal semiconductor layers on a single-crystal substrate. Etymologically, epi means on or on top and taxis means arrangement (from Greek). Thus, epitaxy is the arrangement of

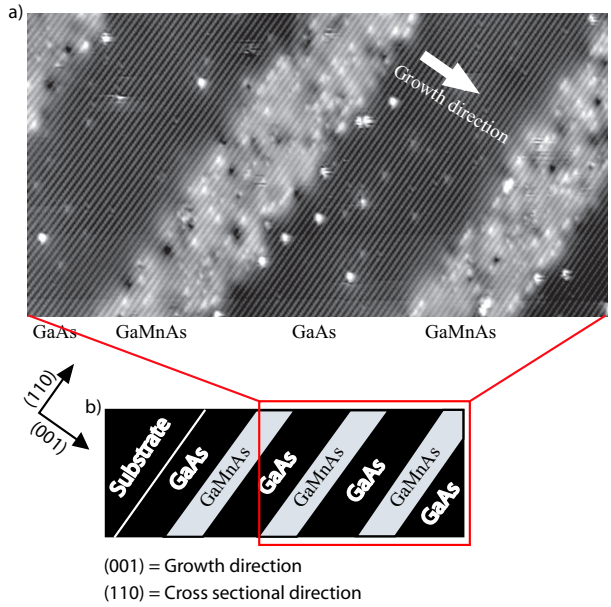

Figure 2.4: a) STM image of a $GaAs/Ga_xMn_{1-x}As$ heterostructure b) model of the $GaAs/Ga_xMn_{1-x}As$ heterostructure. Note: The STM image shows As atoms; the Mn atoms are seen as bright protrusions.

a single-crystal layer on a single-crystal layer (the substrate). The epitaxial layer and the substrate material may be the same. The process is then called homoepitaxy. An example is the epitaxial deposition of a GaAs layer on a GaAs substrate. Heteroepitaxy is the growth of heterostructures in which the epitaxial layers have different chemical and crystallographic structures. For example, the sequential epitaxial growth of $Ga_xMn_{1-x}As$/GaAs shown in Fig. 2.4.

Epitaxial techniques can be classified into three groups depending on how the growth occurs: liquid phase epitaxy (LPE), vapor phase epitaxy (VPE) and molecular beam epitaxy (MBE). In liquid phase epitaxy the materials to be grown are dissolved in a solvent and a supersaturated liquid is precipitated to the substrate. In vapor phase epitaxy the growth material is supplied in gas form; the growth occurs from chemical reactions on the growth surface. Molecular beam epitaxy uses beams of molecules that are evaporated on to the growth surface. MBE and VPE, and closely related techniques like CBE or MOVPE are commonly used epitaxial techniques.

In molecular beam epitaxy beams of atoms or molecules are generated by effusion cells and evaporated onto a crystalline surface (wafer). The effusion cells consist of a crucible in which the material to be evaporated is placed. The crucibles must be thermally stable and non-reactive with the elements to be evaporated since that will be critical for a successful crystal growth. Crucibles of pyrolytic boron nitride are suitable for MBE growth of III-V compounds. It is also common to use a so-called cracker source, which consist of a hot zone

(1000^oC) in front of the arsenic tank to reduce As_4 to As_2 in, for example, growth of GaAs. Furthermore, liquid nitrogen is used to cool the walls of the growth chamber. Hence atoms impinging directly from the evaporation sources reach the substrate (ideal case). Desorbed atoms or atoms that do not reach the substrate are condensed on the walls of the chamber and the background pressure is decreased. After deposition of the desired elements reactions occur on the wafer and the single crystal layer is formed. MBE is operated under ultra high vacuum conditions (10^{-9}torr during operation) with a substrate temperature range of 200-900°C. It can achieve a precise control of the chemical compositions as well as doping profiles. MBE is a suitable technique for fabrication of precise semiconductor heterostructures, but the growth rate is low compared to VPE.

VPE is an epitaxial deposition technique that uses halides (GaCl, InCl, $SiCl_xH_{4-x}$) of group III elements and hydrides (AsH_3,PH_3) of group V elements as precursors. It is an exothermic process which needs hot wall reactor cells to avoid deposition of the gases on the reactor cell walls but preferentially on the substrate. The epitaxial layer is formed by a chemical reaction between the involved gas compounds. The quantum dots and nanowires investigated in this thesis are grown using a special VPE technique, called Metalorganic Vapor Phase Epitaxy, (MOVPE). MOVPE is based on pyrolytic reactions, where the chemical reaction is induced by heating the gases to 500-800°C above a substrate placed on a graphite susceptor. A fundamental difference between MOPVE and conventional VPE lies in the chemical nature of the precursors; metalorganics are used as precursors in MOVPE. In contrast to VPE, the chemical reactions in MOVPE are endothermic using a cold wall reactor cell –only the substrate is heated. In MOVPE molecules containing the atoms to be deposited are transported by a hydrogen or nitrogen carrier gas to the surface where the reaction takes place. After decomposition of the molecules the atoms diffuse across the surface and arrange themselves to form a continuous epitaxial layer. An advantage of using metalorganics in this technique is that they are volatile at moderately low temperatures. For detailed description of epitaxial growth techniques see ref [5].

An important issue in crystal growth is the matching of the lattice constants (distance between the atoms of the crystal) between the substrate and the deposited material in order to increase the number of material combinations. Since the epitaxial layer and the substrate have the same lattice constant in homoepitaxy, by definition homoepitaxy is a lattice-matched epitaxial process (Fig. 2.5a). In heteroepitaxy, the lattice constants of the two materials are either lattice-matched as in $In_{0.53}Ga_{0.47}As$/InP or mismatched as in InAs/InP. In the case of lattice mismatched- or strained-layer epitaxy, the epi-layer will have to accommodate to the substrates lattice spacing. If the epitaxial layer has a larger lattice constant than the substrate, it will be compressed in the plane of growth to conform to the substrate spacing. Thus, elastic forces induce a dilation in a direction perpendicular to the interface as illustrated in Fig. 2.5b. But if the epitaxial layer has a smaller lattice constant than the substrate it will be dilated in the plane of growth and compressed in a direction perpendicular to the interface. In strained-layer epitaxy, as the strained-layer thickness increases, the total number of atoms under strain or the distorted atomic bonds increase. At a certain thickness misfit dislocations are nucleated to relieve the homogenous strain energy. That particular thickness is referred to as the critical layer thickness for the system. Fig. 2.5c shows for example misfit dislocations at the interface.

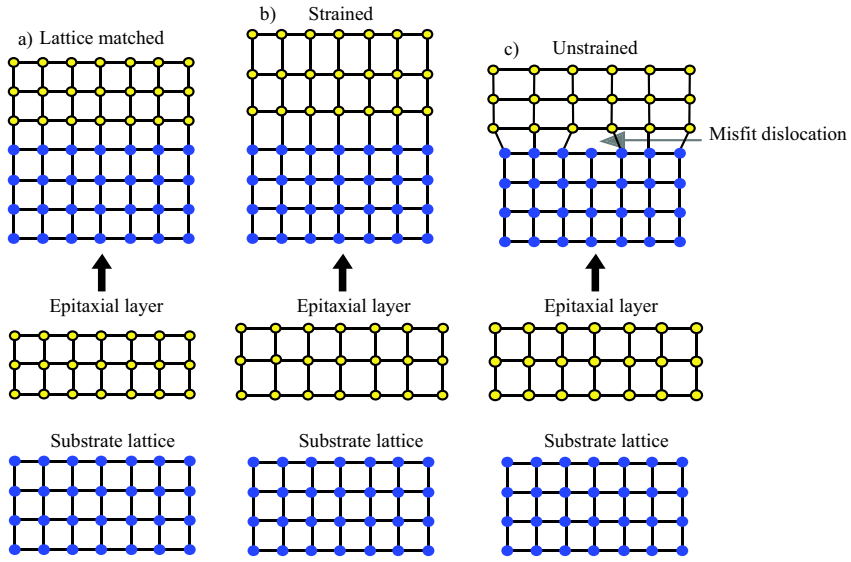

Figure 2.5: Schematic illustration of a) lattice matched structure, b) strained structure, and c) relaxed heteroepitaxial structure with misfit dislocation.

2.3.2 Growth modes

Depending on the amount of incorporated strain in the crystal or the anisotropy of growth different growth modes can be observed:

Frank-van der Merwe growth

When the sum of the substrate surface energy (γ_{sub}) and the interface energy (γ_i) is less than the epi-layer energy (γ_{epi}), it is energetically favorable for the deposited material to cover the surface. Relatively large thicknesses of epi-layers can be grown in a pure two dimensional layer-by-layer fashion with lower surface energy than the original substrate surface. This growth mode is called the Frank-van der Merwe growth mode [52].

A nice example of layer-by-layer growth is shown in Fig. 2.4. Here, alternating layers of GaAs and $Ga_xMn_{1-x}As$ has been grown producing a so-called superlattice or 2D structure. The experimental XSTM image (Fig. 2.4) clearly confirms the smooth layer-by-layer growth of the structure.

Volmer-Weber growth

If $\gamma_{sub}+\gamma_i > \gamma_{epi}$, it is no longer energetically advantageous to wet the surface. The deposited material will directly form three dimensional structures on the bare substrate surface in order to release strain energy, and thereby minimize the energy of the crystal. This is called Volmer-Weber growth [53].

Stranski-Krastanow growth

In the Stranski-Krastanow [54] regime $\gamma_{sub} + \gamma_i \simeq \gamma_{epi}$. At a lattice mismatch of approximatively 2-10% between substrate and epi-layer dislocations are introduced in the layers or the formation of islands, reflecting the incorporated strain due to the lattice mismatch after a certain thickness of epi-layer. The strain in the material increases linearly with the epi-layer thickness up to the critical thickness. At the critical thickness there will be a transition from a pure two dimensional growth to a three dimensional island formation. It is a consequence of the fact that the strain energy cannot be accommodated anymore and it is energetically favorable for the crystal to rearrange by forming three dimensional islands on top of a thin epi-layer. The thin epi-layers are called wetting layers and the islands are often called quantum dots.

Growth mechanism for nanowires seeded by a particle

The growth of the nanowires I have studied is seeded by metal particles (gold particles in our case). The growth mechanism thus differs from the epitaxial growth modes mentioned above. The mechanism is based on an anisotropic crystal growth induced by the metal particle that acts as a local catalyst. The function of the local catalyst resumes in collecting material from the environment (the particle/wire interface acts as a sink in supersaturation), in enabling transfer of material towards the interface (liquid phase or solid phase diffusion transport), and in enabling incorporation of material at the interface (nucleation and growth at a commonly low-energy surface).

Depending on the state of the metal particle, two growth mechanism are found in vapor phase epitaxial growth of nanowires: the vapor-liquid-solid (VLS) mechanism and vapor-solid-solid (VSS) mechanism. In VLS growth as first proposed by Wagner and Ellis [55], the metal particle forms a liquid solution with the growth material at the growth temperature. This condition is necessary in order to create supersaturation which is the driving force for crystallization of the nanowire crystal. In the recently reported VSS growth mechanism the metal particle does not or cannot form a liquid alloy with the growth material [56, 57, 58]. The solid metal particle acts as a collector of materials and provides a low-energy interface for the nanowire growth. The growth mechanism of the present GaAs nanowires has not been established but it is believed to be a VSS growth.

Chapter 3

Scanning Tunneling Microscopy (STM)

The scanning tunneling microscope (STM) was invented in 1982 by G. Binnig, H. Rohrer, Ch. Gerber, and E. Weibel at the IBM Zurich Laboratory. Their ingenious idea was triggered by the observation of vacuum tunneling of electrons between a sharp tungsten tip and a platinum surface. Taking advantage of the ability of raster-scanning the tip over the surface in combination with their finding the scanning tunneling microscope could be developed. Binnig and Rohrer were awarded the Nobel Prize for Physics in 1986 for the invention of STM.

This chapter presents the fundamentals of STM, the experimental setup used in this thesis followed by a description of the tip and sample preparation. Thereafter, cross-sectional STM (XSTM) and imaging of semiconductor surfaces and nanostructures is explained.

3.1 Fundamentals of STM

3.1.1 Principles of operation

Fig. 3.1 illustrates the basic principle of the Scanning Tunneling Microscope. In the microscope a sharp metallic tip often made from a pure metal (tungsten, iridium) or a metal alloy (platinum-iridium) is brought into close proximity to a conducting sample surface. When the separating distance between tip and sample is small enough, typically 0.3-1 nm [59] , there will be an overlap of the tip and sample wave functions. Therefore, electrons start tunneling between tip and sample. At equilibrium no net current will result from the quantum mechanical motion of the electrons. However, if a bias is applied between the tip and the sample, more electrons will tunnel in one direction (tip to sample or sample to tip) depending on the bias. Consequently, a tunneling current is created between the tip and the sample. The resulting tunneling current, I, can be approximated by the following expression [59]:

$$I \propto exp\left(-2d\frac{\sqrt{2m\Phi}}{\hbar}\right) \tag{3.1}$$

where d is the separating distance between tip and sample, m the electron mass, Φ the height of the vacuum barrier, and $\hbar$ Plancks constant. The approximated expression of the tunneling

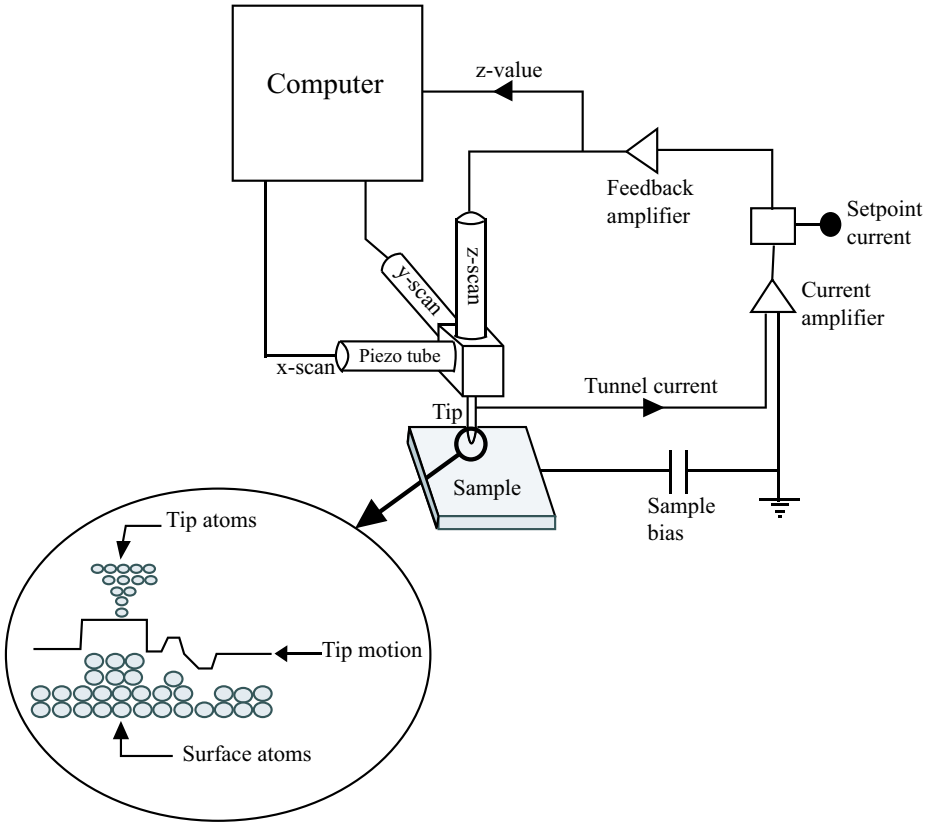

Figure 3.1: Schematic illustration of the principle of an STM setup.

current contains the essential idea of the relatively simple STM technique. Since the tunneling current is an exponential function of the tip-sample separation, for 0.1 nm decrease in the tip-sample separation the current increases by a factor of about 10 [60]. With that level of sensitivity the tunneling current can be used to accurately control the tip-sample separation, yielding a vertical resolution of typically 0.01nm.

The scanning tunneling microscope is most commonly operated in two modes: constant current mode and constant height mode, the first being the most popular. The constant current mode operates by maintaining a constant tunneling current while raster-scanning the surface. This is achieved by a feedback which regulates the tunneling current with respect to a pre-set-point of the current. To maintain the preset current value the position of the tip will then be adjusted by the feedback circuitry. The applied height adjustments of the tip is monitored as a function of the lateral parameters x and y. Consequently, a topographic image of the surface is obtained via a computer.

One example recorded by one of the STMs used in this thesis is shown in Fig. 3.2 where islands of Co on a Mo substrate are imaged. Fig. 3.2b also shows an image displaying atomic resolution on a Co island [61].

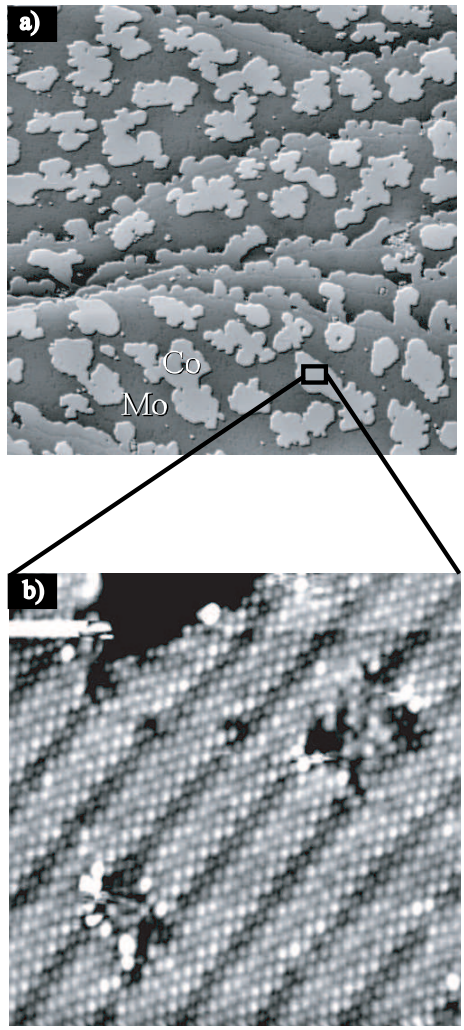

Figure 3.2: a) STM image of Co islands on a Mo substrate b) a zoom-in on a Co island, displaying the Co atoms in the island [61].

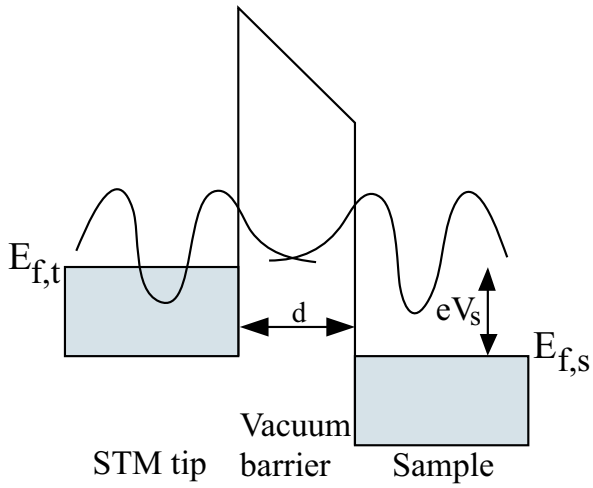

Figure 3.3: Schematic illustration of the tunneling process between tip and sample for a positive sample bias V_s. The different overlapping wave functions are indicated.

In the second mode of operation (constant height mode) the feedback system maintains a constant tip height above the surface during the scanning process. The current fluctuations then generate the image. However, that method is used less because it requires greater stability of the measurement setup and flatter surfaces [59, 60, 62].

3.1.2 The joy of tunneling in STM

When I was a young boy, my grandmother used to tell me fairy tails. But one day she told me a story that she claimed was true. There was a strange village in the deepest forest of Africa, a village of Djins. In that village the Djins were living in big Baobab trees without holes or doors and they could move through these big trees! For very long time in my life I have been thinking about what my grandmother said that day and how that could be possible! Then, when I started learning quantum mechanics, I realized that my grandmother forgot or omitted to mention that these Djins were like electrons. They have the power of tunneling through a barrier!

STM is a powerful imaging technique because of its ability of producing direct images of different surface features with a resolution on the atomic scale (under favorable conditions). In order to understand the topographic imaging of STM a quantum mechanical theory of the tunneling phenomena in STM has been developed.

In the 80s Tersoff and Hamann [63, 64] presented a theoretical description of STM that offers a straightforward explanation of the physics of STM. The complete description of their theory is based on a earlier work published by Bardeen in 1961 [65]. Tersoff and Hamann considered the overlap of the two independent wave functions of the tip and the sample (Fig. 3.3). Assuming a weak interaction between tip and sample and a low gap voltage, they used a first-order pertubation theory to describe the tunneling current between the tip and sample. Using Bardeens transfer Hamiltonian approach [65], the tunneling current can be

written as:

$$I = \frac{2\pi e}{\hbar} \sum_{s,t} f(E_t) \left[1 - f(E_s + eV)\right] |M_{st}|^2 \delta(E_t - E_s), \tag{3.2}$$

where $f(E)$ is the Fermi-Dirac distribution function, V the applied voltage, and M_{st} the tunneling matrix element between states ψ_t of the tip and ψ_s of the sample, E_t and E_s the eigenenergies of the tip and the sample, respectively. Following the derivations of Bardeen the tunneling matrix element is given as a surface integral evaluated over any surface lying entirely in the vacuum (barrier) region.

$$M_{st} = \frac{\hbar^2}{2m} \int d\vec{S}.(\psi_t^* \vec{\nabla} \psi_s - \psi_s \vec{\nabla} \psi_t^*) \tag{3.3}$$

where the quantity in parentheses is the current density and m the electron mass. It turns out that only electrons near the Fermi level contribute to the tunneling at low temperatures and low gap voltages [63, 64]. In order to calculate the tunneling current the wave functions of the tip and sample have to be known. Since the geometry and actual atomic structure of the tip is in general not known, an explicit evaluation of the tip wavefunction is a limiting factor. Tersoff and Hamann approximated the tip wavefunction with an s-wave and assumed the end of the tip to be a sphere of radius of curvature R and center r_o. They could then derived the following expression for the current:

$$I \propto \sum_s |\psi_s(r_o)|^2 \delta(E_s - E_F) \equiv \rho(r_o, E_F) \tag{3.4}$$

This result shows that the tunneling current is proportional to the surface local density of states (LDOS) at the Fermi level. Hence, a constant current topograph from an STM is essentially a contour map of constant surface LDOS at the Fermi level. Tersoff and Hamann's theory was shown to be successful for calculations of (2x1) and (3x1) reconstructions of Au(110) and also for predicting the voltage dependent imaging of GaAs(110) surfaces by Feenstra and Stroscio [66].

Today advances in contemporary ab-initio theory and modeling combined with the computing power of today, make simulations of STM images a powerful atomic structural technique if compared to experimental STM images [67]. Recent developments in STM theory also takes into account the precise shape of the tip using ab-initio density functional theory (DFT) methods [67].

We have successfully used the Tersoff and Hamann's theory to simulate the expected appearance of Mn at different sites in the GaAs (110) surface. By comparing the theoretical simulations to the experimental observation, we can deduce the location of the Mn atom.

3.2 Experimental setup of the STM

3.2.1 Apparatus

The experimental setup for an STM is often determined by the scope, the thermal, and chemical environment of its use. For applications in surface science and nanoscience, like investigations of surface structures and chemistry or structural studies of nanostructures, the instrument is suspended in a soft damping system in an ultra high vacuum (UHV) chamber.

Since vibration is a critical issue in STM experiments, limiting a successful operation of STM, despite the suspension of the STM in a damping system, the UHV chamber with the analytical instruments is mounted on a table, which is also isolated from vibrational motions from the laboratory floor and neighborhood. Furthermore, an experimental limitation for an STM is the requirement of conducting surfaces in order to obtain a tunneling current.

The experimental setups used for this thesis are a commercial tripod and tube scanner Omicron STM operated at room temperature. The UHV system to which the STM is connected operates at a base pressure below 3×10^{-10} mbar allowing for 1-3 days of measurements, depending on the studied surface, before significant contaminations are observed. Fig. 3.4 shows a photograph and a schematic illustration of one of the systems. It comprises two chambers: the preparation chamber and the analysis chamber. In the preparation chamber the samples and tips can be cleaned. In the analysis chamber the samples are cleaved and studied using STM. In order to insert the samples into the UHV-system, a load-lock entry is available. The load-lock compartment, the preparation chamber and the analysis chamber are all separated by valves for fast sample transfers and to maintain a good vacuum pressure inside the system. In addition, the system contains equipment for Auger Electron Spectroscopy (AES) and Low Energy Electron Diffraction (LEED) measurements. The main difference between the tripod and tube scanner instrument, except for the fact that the tube configuration is compact and have higher resonant frequency, usually 12 to 20 kHz, is on the design and scan-range.

3.2.2 Tip and sample preparation

The requirements on the tip in an STM measurement varies according to the applications. For a flat surface, looking at very small structures, the shape of the tip is of no great importance except that it should end by a single atom. When looking at larger scale features where the surface cannot be considered as flat, the tip has to have a small cone angle. This requirement is due to the fact that the tip should be able to penetrate into very narrow gaps at a surface. However, in general the exact geometry of the tip is not known except for non-standard STM experiments, in which the structure of the tip is determined before and after a scan by field-ion microscopy [68].

Tips can be made of different materials, also depending on the desired application and in what environment it is supposed to operate. One main requirement when choosing the tip material is that it has to be of hard material which better copes with non-intentional contacts between tip and sample. The chemical reactivity and surface diffusivity are also important parameters when choosing a tip material. Noble metal tips such as gold or platinum are less sensitive to contaminations compared to easily oxidized metals like tungsten. Furthermore, more reactive tip materials enhance the interaction between tip and sample atoms which affects the achievable resolution during measurements. Since the quality of STM images depends on the arrangement of a single atom or small number of atoms, surface diffusion of the atoms could cause abrupt changes in the image quality. A tip will therefore be more stable if the active atom at the tip apex is tightly bound to the tip surface. For uses in ultra high vacuum, pressures below 10^{-8} torr, a tungsten tip is usually chosen because tungsten is a hard material and one also want to avoid their oxidation. In conditions with higher pressures Pt-Ir alloys are commonly used. Probing III-V semiconductor based structures, UHV conditions are needed to keep the surfaces clean and prevent oxidation. It is therefore common to use a

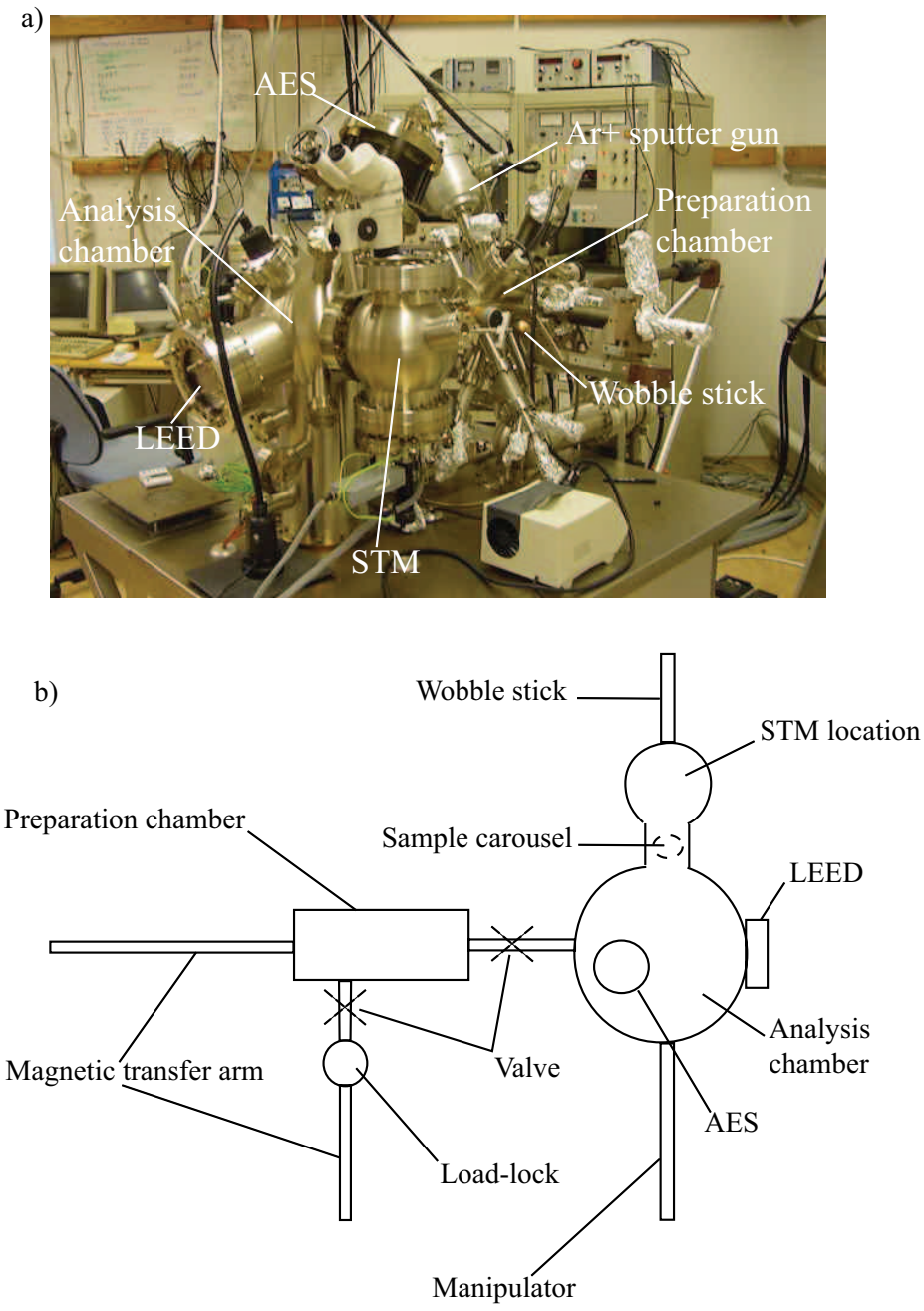

Figure 3.4: The UHV system with the scanning tunneling microscope used in this thesis: a) photograph of the system, b) schematic illustration of the system.

tungsten tip in that case.

The tips used in this thesis are made by electrochemical etching of a thin polycrystalline tungsten wire. A home made DC-etching setup is used. To get the tip as sharp as possible the wire is immersed vertically (approximatively 3 mm) in a 2M KOH solution. Since the chemical reaction is faster at the meniscus formed between the wire and the surface of the solution, the wire breaks at that contact point due to gravitational forces. As soon as the wire breaks, the applied DC-voltage is automatically switched off and the tip is removed from the solution to avoid tip bluntening. During the etching a thin oxide layer is formed at the tungsten surface. Once the tip is brought into the UHV chamber, this oxide layer is removed by ion beam sputtering.

The preparation of the surfaces is done using different methods depending on the material system in question and the scope of the measurements. What always matters when preparing a surface to be studied by STM is that it should be reasonably macroscopically flat. This is because the tip motion is limited by the range in which the piezoelectric scanner can be operated. It is also important that the surface is clean in the sense that what is to be studied cannot be covered by any other atoms since the STM only sees the outermost atomic layer. Note also that rough and uncleaned surfaces can cause unstable tips. See also section 3.3 for complementary information on the sample preparation.

3.3 Cross-sectional STM (XSTM)

3.3.1 Introduction to XSTM

Although STM is a powerful probe technique, it only enables a characterization of the topmost atomic layers of a sample. In order to explore buried structures in III-V semiconductors an STM technique called cross-sectional STM (XSTM) can be used [69]. The basis of XSTM is the same as for normal or conventional STM. XSTM is characterized by the fact that the samples are cleaved to expose a cross-sectional surface of the crystal. Fig. 3.5 illustrates the different steps of an XSTM experiment. The technique is especially used for characterization of III-V semiconductor-based structures such as the structures studied in this thesis. Since the (110) plane of the III-V crystals has the lowest surface energy, the preferential cleavage direction of those samples are the [110] and [1-10] directions.

When cleaving the crystal former bulk atoms become surface atoms. Since the neighborhood of these atoms have changed drastically, they will experience a new ”landscape”. Consequently, a relaxation of the atoms occurs. This relaxation can be small resulting in a change in the distance between the atomic layers. It can also be more drastic, resulting in a redistribution of the atoms.

3.3.2 Experimental details

Before mounting a sample on the sample holder a small notch is made on the sample. The notch initiates the cleavage at a specific position. When the sample is introduced into the UHV system, it is Ar^+ ion beam sputtered followed by an annealing in order to clean it and avoid that impurities diffuse to the cleaved surface. The cleavage is done *in-situ* by a gentle touch of the sample with the wobble stick.

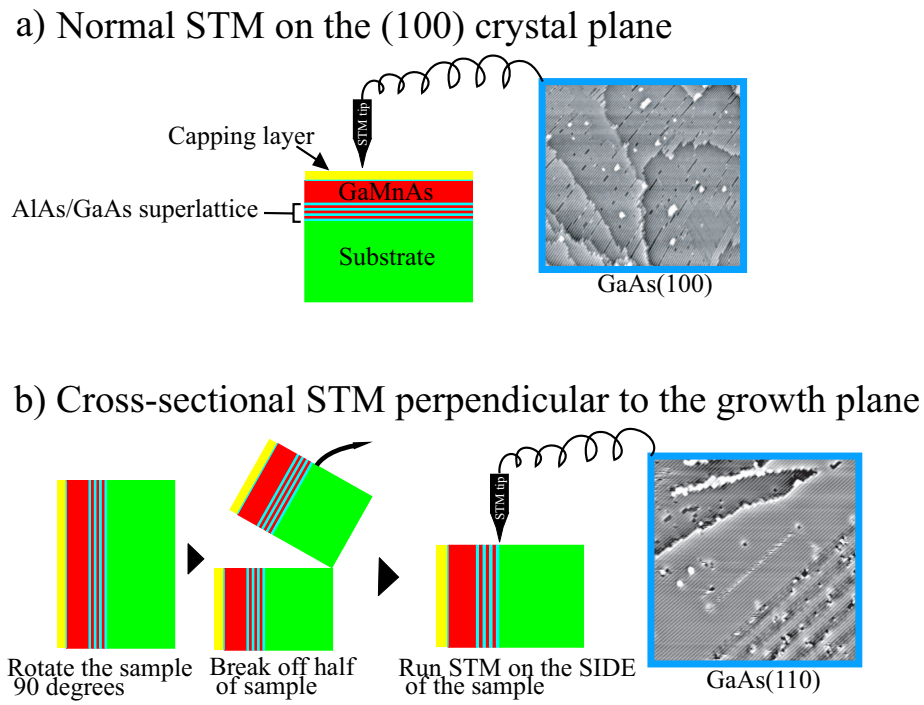

Figure 3.5: a) the tip is being scanned on the (100) plane meaning that the structure can not be seen, b) the sample is first rotated 90 degrees and then cleaved. It is now possible to scan a structure of interest.

Starting the measurement, I first make a rough positioning of the tip on the substrate using an optical microscope or a CCD-camera as used in our new system. After the approach at this position I find out if the cleavage was performed somewhat satisfactorily. If this is the case, the tip is moved very close to the edge of the sample toward the capping layer, again using the optical microscope or CCD-camera. A new approach is then done and the tip is moved toward the edge of the sample using a stepwise procedure. The lost of contact between tip and sample indicates that the tip is positioned beyond the edge of the sample. By returning onto the sample using a stepwise procedure, each step corresponding to roughly 200 nm, the buried structures can be found. Looking for buried structures in this way is challenging and time-consuming, but very exciting. Once a searched structure is found, the next challenge is to obtain atomically resolved images on it. This is a process which is not straightforward due to the strong dependence of STM measurements on the quality of the tip. However, with a "corporating" tip the local atomic-scale geometry of such structures can be visualized. XSTM has a number of unique features compared to other structural characterization methods for buried nanostructures such as cross-sectional transmission electron microscopy (XTEM). The most important one is probably the possibility with XSTM to obtain images displaying atomic resolution of individual atoms and point defects in a structure. In contrast to XSTM which probes individual atomic features, TEM images average over many hundred atomic planes in the direction perpendicular to the image plane. Thus, TEM

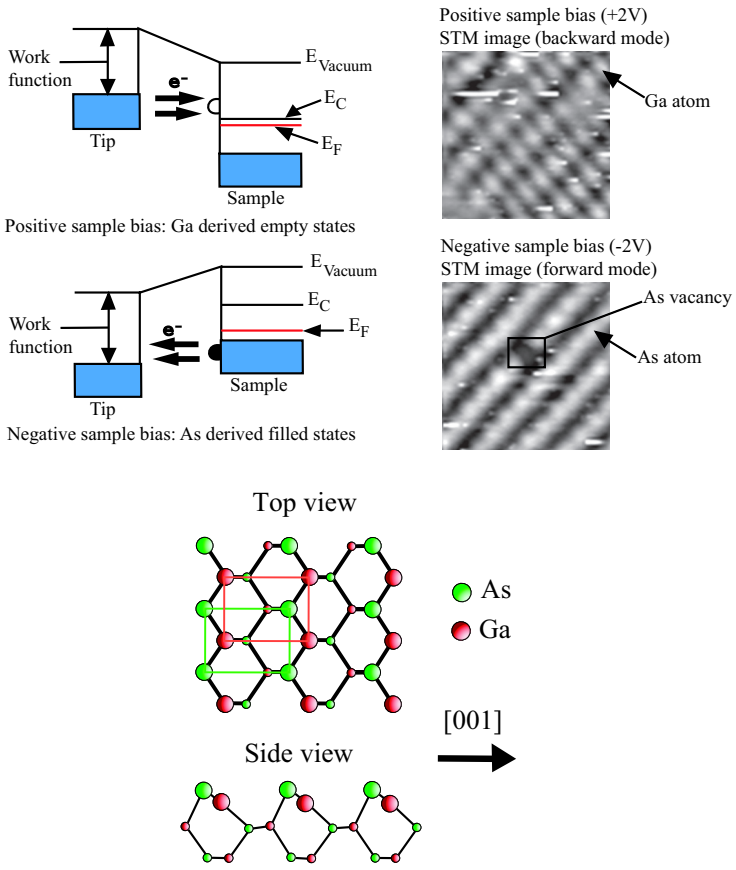

Figure 3.6: Illustration of bias-dependent imaging for GaAs (110). The two STM images are from the same sample area and have been taken simultaneously in forward (negative sample bias) respectively backward (positive sample bias) mode.

and XSTM measurements are in many ways complementary. For nanoscale structures, such as complex superlattices, nanowires and quantum dots, this means that it can be difficult to attribute the defects being imaged to a specific local site inside the structure without using STM.

3.3.3 Imaging the GaAs(110) surface with STM

The atoms in the III-Vs form a cubic lattice, more specifically they are arranged in the zincblende structure. The III-Vs are covalent crystals, meaning that the bonds between the atoms of different kinds are covalent bonds. In a covalent III-V crystal the valence electrons are distributed so that there is slightly more of the electron cloud around the group V atoms than the group III ones to compensate for the higher positive charge in the nucleus. Therefore, the negative charge around the group III atoms is also correspondingly less. This is an

important point when imaging III-Vs by STM since that induces a possibility to distinguish between the group III atoms and the group V atoms in the lattice.

To illustrate the appearance of (110) III-V surfaces in XSTM the GaAs (110) surface can be used. However, similar arguments are also valid for other III-V (110) surfaces. A model of the GaAs (110) surface is shown in Fig. 3.6, where the topmost atoms are arsenic (As) atoms and the gallium (Ga) atoms are in the layer just below. Investigating such a surface by STM using a negative bias results in an image as shown in Fig. 3.6. The tunneling current in this case arises from the electron flow from the filled states located at the As sites into the tip, and consequently the protrusions in the image can be attributed to the top-most As atoms. When a positive bias is applied the tunneling electrons will flow from the tip into the empty states located at the Ga atoms, yielding an STM image as shown in Fig. 3.6. Here the protrusions are therefore related to the Ga atoms. The first XSTM measurements on a GaAs (110) surface was reported in 1985 [69] and the ability to chemically distinguish between the Ga and As atoms by changing the tunneling bias was realized shortly thereafter [66].

3.3.4 Probing embedded QDs by XSTM

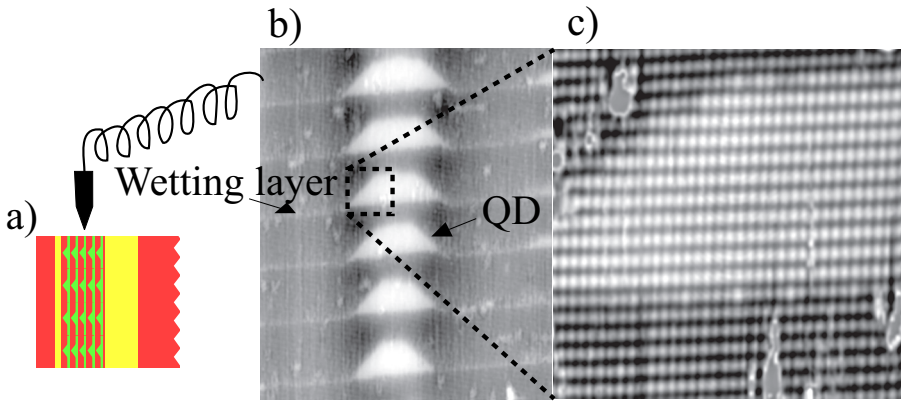

Figure 3.7: a) The tip is being scanned on the cleaved (100) crystal plane, b) XSTM image of a cleaved QD sample, c) InAs QD with atomic resolution.

Fig. 3.7b shows a typical XSTM image of one of our studied QD samples. In this figure a set of five stacked InAs QDs grown in InP is presented. The brighter protrusions in the image are the InAs QDs lying on less bright horizontal lines which are the wetting layers. Once an overview image of the structure is obtained the next step is to zoom in on a QD in order to view inside it. Thus Fig. 3.7c presents an XSTM image where I image inside a selected QD. The image shows atomic rows of arsenic (As) atoms on the QD and phosphore (P) atoms on the surrounding layers. The fact that it is the As and the P atoms which are probed using negative sample bias was explained in subsection 3.3.3. Due to geometrical and electronic effects the atomic rows on the QD appear brighter compared to the atomic rows on the surrounding InP layers. Moreover, many different features can be visualized using XSTM to explore buried QD structure, in particular different defects and growth artifacts. The reader is referred to the related enclosed papers for more details. However, an XSTM

measurement on a QD structure also contains severe difficulties with respect to the cleaving procedure.

Since the dots are randomly distributed on the surface, the cleavage plane of the QDs is in principle random. Consequently, one has to be careful when estimating the size distribution or establishing the exact shape of the dots. However, that problem can be solved in the case of stacked QDs as demonstrated in paper III.

The most commonly studied QD system using XSTM is InAs QDs in a GaAs matrix [70, 71, 72]. These studies have been able to determining the vertical alignment, the chemical composition, the strain field as well as the shape of the dots. It has in particular been found that In has a strong tendency to diffuse in the GaAs lattice in that system, while the same tendency is not observed in the present InAs/InP system.

3.3.5 Probing embedded nanowires by XSTM

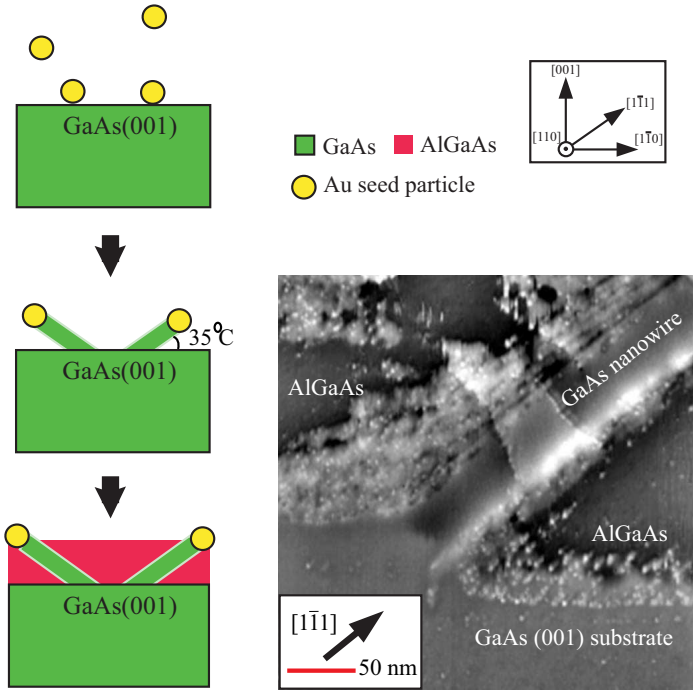

Figure 3.8: a) schematic of the embedding scheme; b) XSTM image of GaAs nanowire encased by AlGaAs (300x300 nm^2, U = -2 V, I = 0.1 nA).

The properties of nanowires can be considerably affected by individual atomic scale features since nanowires have a large surface to bulk ratio and a small cross section. Hence structural investigations of nanowires on the atomic scale are of great interest. High resolution electron microscopy (HRTEM) measurements showed very impressive results on the average atomic scale-structure through nanowires, thus characterizing crystal structures and

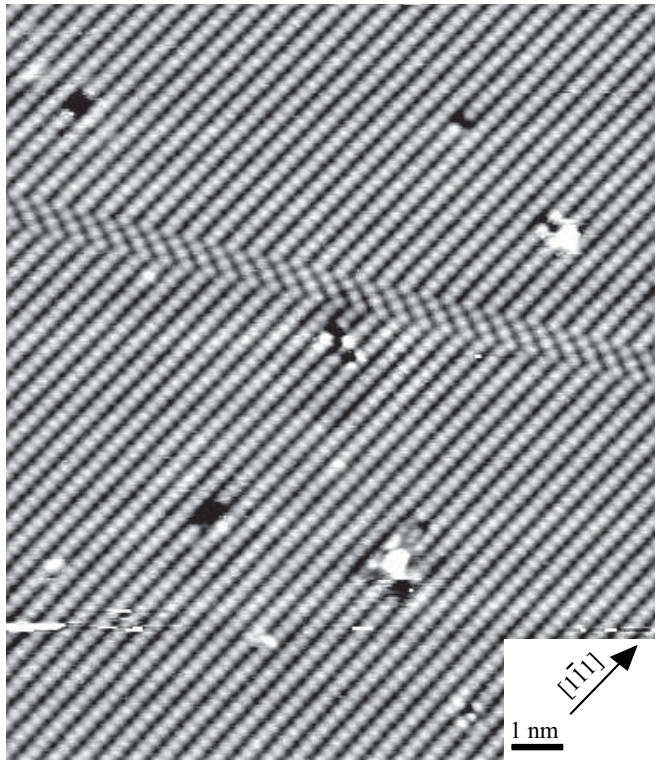

Figure 3.9: Atomically resolved XSTM image (U = -2 V, I = 0.1 nA) inside a nanowire containing a stacking fault.

heterostructures along the wire. HRTEM is the standard tool used for structure and morphology characterization of nanowires. However, to obtain atomic scale information on the nanowires, STM and XSTM is a good complement to HRTEM. Additionally, XSTM can image the bottom part of the wire near the wire/substrate interface, while HRTEM usually images the top of the wire near the Au seed particle. In order to be able to perform XSTM on free standing nanowires, we have used a special crystalline embedding scheme which does not influence the experimental results. By embedding the III-V nanowires in a lattice matched ternary III-V alloy, we can cleave the wire sample. STM measurements can then be performed on the cleaved surface of the wire and surrounding material.

Fig. 3.8 shows the crystalline embedding scheme and a typical XSTM image of an embedded nanowire and the surrounding GaAs and AlGaAs material. As in all XSTM measurements, once the structure is identified, one can zoom in and view inside the structure as shown in Fig. 3.9. However, as in the case of QDs described above or the GaMnAs thin film describe next, finding the wires and achieving atomic scale resolved images on it is not straightforward. The method I use is to find the interface between the GaAs substrate and the AlGaAs embedding material. Subsequently, the GaAs/ AlGaAs interface is followed until the base of a wire is found. Two main features are decisive for the success of the experiment.

One has to avoid large cleavage induced steps and it is good to have high enough wire density in order to find any wire. However, as the structural defects and heterostructures of the wires induces step formation at cleavage, it is at the same time desirable to have as low wire density as possible to avoid these steps formation at cleavage. The other issue is that the growth is generally complicated by a high density of wires, as the wires may influence each other or can even attach to each other during growth. With decreasing wire density the chances of finding a wire within a reasonable time also decreases dramatically. Hence XSTM on nanowires is not an easy task!

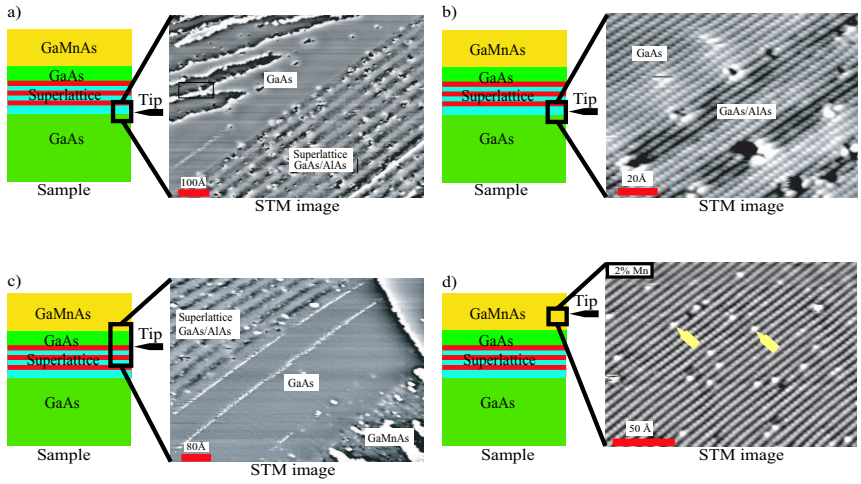

Figure 3.10: Finding the $Ga_xMn_{1-x}As$ layers, a) identifying the superlattice (SL) structure, b) atomic resolved image on SL/substrate, c) identifying the $Ga_xMn_{1-x}As$, d) zoom in on the $Ga_xMn_{1-x}As$. Note: The arrows in Fig. 3.10d indicate Mn atoms.

3.3.6 Probing $Ga_xMn_{1-x}As$ by XSTM

Fig. 3.10 illustrates a search for a buried $Ga_xMn_{1-x}As$ thin-film. The sample structure consist of a GaAs substrate followed by a 7 ML ($\sim$ 2 nm) AlAs/GaAs superlattice, approximately 200 nm GaAs and then the $Ga_xMn_{1-x}As$ (0.5 μm) layer buried between the 200 nm GaAs and 0.5 μm GaAs capping layer. In Fig. 3.10a the AlAs/GaAs superlattice is identified, with a sharp interface separating the GaAs substrate to the superlattice. Once such an image is obtained using the procedure described in 3.3.2, one can zoom in and get an image displaying atomic resolution of the superlattice as shown in Fig. 3.10b. Having identified the superlattice, the search for the $Ga_xMn_{1-x}As$ layer is done by moving stepwise toward the capping layer. Hence, in Fig. 3.10c I imaged part of the AlAs/GaAs superlattice, the subsequent GaAs and the $Ga_xMn_{1-x}As$. Once the desired structure ($Ga_{0.98}Mn_{0.02}As$) is identified, it can be studied on the atomic scale in great detail (Fig. 3.10d).

Fig. 3.11a presents images displaying atomic resolution of both filled state (negative sample bias) and empty state (positive sample bias) of the GaMnAs layers. In the filled state image the As atoms are imaged while the Ga atoms can be seen in empty state imaging [66].

By comparing the expected Mn bulk concentration with the number of bright defects in the image, it can be concluded that the bright defects reflect the Mn atoms in the sample. Further, it is obvious from the positive bias image in Fig. 3.11a that this defect is in between the Ga rows. It is rather surprising that the Mn related protrusions appear in between the Ga rows, since it is known from previous studies that the Mn should substitute the Ga atoms. This observation combined with the fact that STM probes the electronic structure rather than the direct atomic positions in the lattice, prompts us to simulate the STM images using the Tersoff-Hamann approach previously described. By comparing the simulated STM images from various structures as obtained by ab-initio calculations, only the structure shown in Fig. 3.11b agrees well with the experimental images.

Surprisingly, no Mn is found in the top-most Ga rows, but instead in the second Ga rows. It is likely that the Mn in the top-most Ga layer can more easily diffuse due to the presence of the surface, consistent with ab-initio calculations. It should be noted, that despite this surface induced diffusion process, the bright protrusions still directly reflect the bulk Mn concentration, a property which has been used to study Mn diffusion in $Ga_xMn_{1-x}As$ superlattices [73, 74].

The $Ga_xMn_{1-x}As$ (110) system is a good example on how to characterize very thin layers of a material with a low density of defects on an unprecedented level using a combination of XSTM and ab-initio DFT calculations [75].

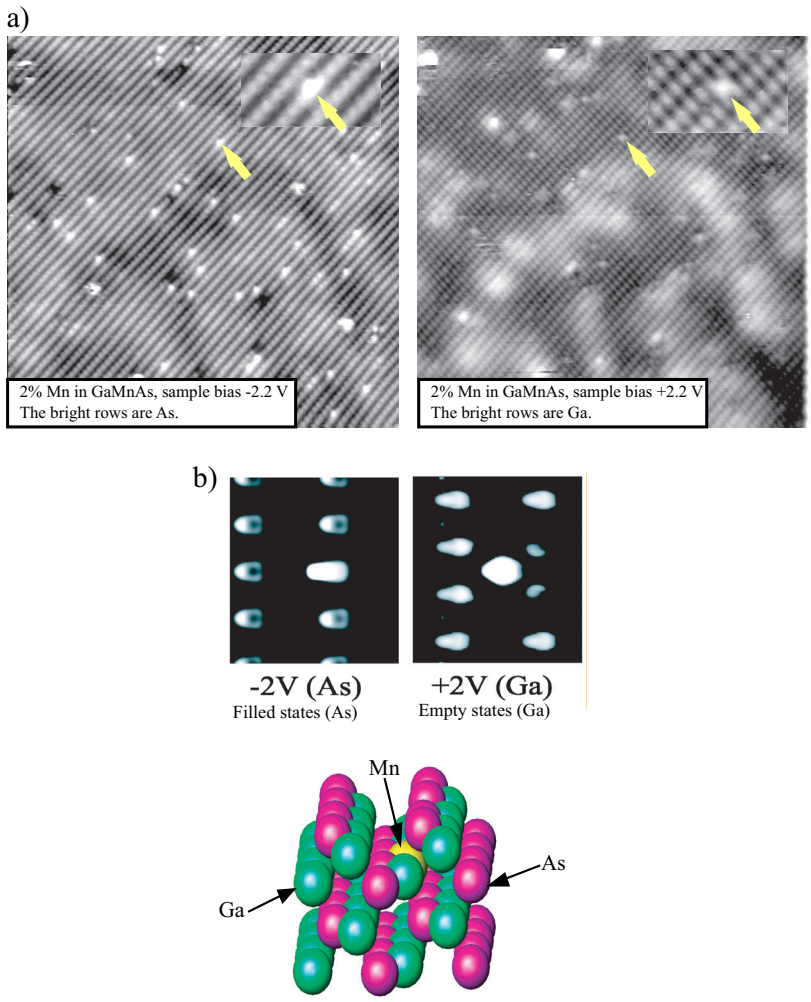

Figure 3.11: a) By scanning the same area with a sample bias of -2.2 and +2.2 V simultaneously one images the As and the Ga rows, respectively. This demonstrates that the Mn related protrusions situates in the As rows and thus in-between the Ga rows. Note: The insets are zoom in of the area around the arrow pointing at a Mn atom, b) simulated STM images and the $Ga_xMn_{1-x}As$ (110) model used.

Chapter 4

Summary of papers

4.1 Semiconductor quantum dots

4.1.1 Paper I: Correlation lengths in stacked quantum dot systems: Experiment and Theory

The influence of the indium phosphide (InP) spacer layer thickness on the vertical alignment of indium arsenide (InAs) quantum dots (QDs) is studied. It is found that the distance at which the vertical correlation of the InAs/InP QDs is lost, is similar to the one of the InAs/GaAs QDs despite the large mismatch difference between the two systems. It has been previously demonstrated that the InAs/InP QDs consist of pure InAs dots with very little intermixing at the outermost dot layers (see 4.1.3) as opposed to the InAs/GaAs QD system [70, 76, 77]. However, here it is demonstrated by theoretical considerations that the difference in alloying properties does not result in a large enough reduction of the lattice mismatch difference between the two systems. Thus, the differences in alloying properties is not sufficient to explain the similar results in both systems. When the QD size is taken into account in addition, the observed similarities can be explained. Thus, both the non-intermixing and the bigger dot sizes in our system compensate for the strain differences in both systems. Further, the present XSTM images show that the strength of the vertical correlation strongly influence the size of the QDs.

4.1.2 Paper II: A cross-sectional scanning tunneling microscopy study of a quantum dot infrared photo-detector structure

In this paper, cross-sectional scanning tunneling microscopy (XSTM) studies of a quantum dot infrared photo-detector structure (QDIP) are presented. The structure was grown by metal-organic vapor phase epitaxy in a vertical Emcore reactor operating at 100 mbars. The structure consist of a modulation doped 10-layer stack, where each period consisted of a 2 nm $In_{0.15}Ga_{0.85}As$ buffer layer, InAs QDs, 6 nm $In_{0.15}Ga_{0.85}As$ cap layer, and a 33 nm GaAs barrier. It was capped by 0.5 μm GaAs in order to avoid cleaving damages during the XSTM experiment.

In the present paper the composition, shape and size distribution of the quantum dots is investigated. It is shown that the quantum dots are strongly intermixed with the InGaAs

quantum well layer and they have a non-uniform size distribution. Their shape could best be approximated to an oval dot shape. Furthermore, defects related to Si-dopants atoms introduced in the structure are identified and their concentration is estimated.

4.1.3 Paper III: Stacked InAs quantum dots in InP studied by cross-sectional scanning tunneling microscopy

This paper presents a more detailed cross-sectional scanning tunneling microscopy (XSTM) investigation on vertically stacked InAs quantum dots in InP surrounded by GaInAs. Two, five, and ten stacked quantum dot structures grown by low-pressure metal organic vapor phase epitaxy are studied. As in the study presented in paper I, the XSTM images reveal that the quantum dots are generally vertically well aligned and have almost pure InAs stoichiometry, with intermixing only occurring in the top and bottom dot layers. The spontaneous formation of an extra quantum dot on top of the buried stacks, at the InP/GaInAs interface is also frequently observed.

Furthermore, the quantum dots have a truncated pyramidal shape with a flat (001) base and top plane, and an inclination angle of 35° is found between the side facets and the base plane. The dots have a constant height but an increasing baselength with dot position up to a certain position, at which the baselength becomes constant. Some defects or growth imperfections like the formation of so-called semiconductor rings, perturbed vertical stacking and morphology changes in the top GaInAs layer are also observed.

The semiconductor rings are quantum dots in which ring-like or hole-like depressions have evolved. Their occurrence is growth temperature related, and they are believed to possess interesting electronic properties [78].

The study also demonstrates that larger quantum dots in a stack can repel smaller adjacent dots, perturbing the vertical alignment of the adjacent stacks -perturbed vertical stacking.

Finally, the study shows that one observes a depression in the top-most GaInAs layer whenever spontaneous extra dots are formed. These depressions are due to the strain field induced by the extra dot.

4.1.4 Paper IV: Spontaneous InAs quantum dot nucleation at strained InP/GaInAs interfaces

Cross-sectional scanning tunneling microscopy (XSTM) is used to investigate a structure with two stacked InAs quantum dots in InP surrounded by layers of GaInAs. The studied structure is grown by low-pressure metal organic vapor phase epitaxy. It is similar to a structure for which resonant tunneling has been demonstrated [20, 21, 22]. It is found that the quantum dots aligned vertically on top of each other due to the strain field induced by lower lying dots. Taking advantage of the XSTM images displaying atomic resolution on the dots, it can be stated that the quantum dots mainly consist of pure InAs with little intermixing of P at the outermost dot layers. A spontaneous formation of an extra InAs quantum dot on top of the previous ones, at the InP/GaInAs interface is also observed. The formation of the extra quantum dot could be explained by the following two phenomena: since In atoms have longer diffusion length than the Ga on the growing surface [79], In could diffuse towards the tensile strained regions with lowered chemical potential above the buried dots during the deposition of the GaInAs. Consequently, a phase segregation occurs in the GaInAs, inducing

an accumulation of InAs just above the stacks, providing enough material for the formation of the extra dot.

It is known that As/P exchange reactions are enhanced at strained regions [80]. Thus, more material for dot formation could be available at the strained areas above the buried dots, inducing the nucleation of the extra quantum dot.

4.2 Semiconductor nanowires

4.2.1 Paper V: Direct imaging of heterostructures inside a nanowire by scanning tunneling microscopy

The potential of semiconductor nanowires in realizing application devices in physics, chemistry and biology relies on the possibilities to design complex nanowire heterostructures with both lateral and vertical material variations [45, 48]. There is a need thus of growing and characterizing perfect nanowire heterostructures down to the atomic scale. In this paper, we present cross-sectional scanning tunneling microscopy results on GaAs/AlGaAs nanowire heterostructures. The high resolution STM images reveal that the initial (bottom) interface between the AlGaAs segment and the GaAs nanowire is very sharp, while the top interface is found to be diffuse, showing a gradual Al concentration which can be related to Al interdiffusion from the Au seed particle. The morphology and composition of an AlGaAs shell surrounding a GaAs core nanowire is investigated, observing even extremely thin shells with thicknesses below 1 layer. Finally, we observe significant structural and morphological defects on the sides of the wires related to areas of twin formation in the wires.

The measurements indicate how the core/shell type of wire growth during wire production can completely eliminate these morphological defects creating wires with an atomically flat surface.

4.2.2 Paper VI: Nanowire growth and dopants studied by cross-sectional scanning tunneling microscopy

Using a crystalline embedding scheme it has been possible to study free-standing III-V nanowires with cross-sectional scanning tunnelling microscopy (XSTM). In the present paper it is discussed how this novel method can be used to probe nanowires with STM, obtaining images displaying atomic resolution of the nanowires. Two of the unique possibilities that this method provides are emphasized. The growth of the nanowires at the substrate as studied by XSTM is discussed and the facets of the nanowire growth on the surface and at the onset of free-standing nanowire growth is determined. This paper also demonstrate how individual defects can be studied inside the wires, thus presenting a unique way for investigating dopant structures and their concentrations in nanowires. A carbon defect/dopant in the nanowire positioned on arsenic sites is identified and quantitative limits on the defect density in the nanowires are established.

4.2.3 Paper VII: Direct imaging of the atomic structure inside a nanowire by scanning tunneling microscopy

Gallium arsenide (GaAs) nanowires grown on a GaAs (001) substrate by metalorganic vapour phase epitaxy are studied by cross-sectional scanning tunneling microscopy (XSTM). The nanowires are embedded in aluminium gallium arsenide (AlGaAs) in order to make the XSTM measurement feasible. The wires grow in the $< 111 >$B direction, with a 35.3^0 angle to the (001) substrate. However, it is often found that the nanowire initially creeps along the (001) substrate in the [1-10] direction before taking off. The STM images show that the nanowires are embedded in crystalline AlGaAs and that it is possible to cleave the sample and obtain an atomically flat cross-section of a wire. Large areas inside the nanowire are virtually defect free, and the wire has the common zinc-blende structure of GaAs. But a number of single defects are observed. Some of these defects are arsenic (As) vacancies that are created after the cleavage by, for example, the STM tip. Other observed defects, as bright protrusions found in the As lattice, indicate that single atom impurities are also present inside the wire. Defect structures such as planar twin segments are also found in the structure.

It is interesting to note that the insertion of twin segments, thus stacking faults inside the nanowires, results in breaking of the wire symmetry, which might have consequences for the electronic properties of the wire.

Further structural details of the nanowire structure can be obtained by cleaving the crystal parallel to the (1-10) plane. Thus, instead of exposing a plane along the wire, a slice through the wire is obtained. As this cross-section intersects the wire at an angle of 55^0, one will observe an elongated hexagonal shape for a perfectly symmetric hexagonal nanowire.

4.3 Dilute magnetic semiconductors

4.3.1 Paper VIII: Mn diffusion in $Ga_{1-x}Mn_xAs$/GaAs superlattices

In this letter a study of $Ga_{1-x}Mn_xAs$/GaAs superlattices with Mn concentrations of 1% and 5% in the $Ga_{1-x}Mn_xAs$ layers and a GaAs spacer thickness of 4 and 60 GaAs monolayers has been performed using cross-sectional scanning tunneling microscopy (XSTM). XSTM images displaying atomic resolution enabled the estimation of the abundance of Mn atoms in the $Ga_{1-x}Mn_xAs$ layers. Individual Mn atoms are identified in the $Ga_{1-x}Mn_xAs$ layers and it is shown that Mn is also present in the non-intentionally doped GaAs spacer layer in amounts proportional to the total Mn content in the $Ga_{1-x}Mn_xAs$ layers. About 20% of the total amount of Mn diffuses from the GaMnAs layers into the GaAs spacer layers.

For short period superlattices, the Mn diffusion into the spacer layer may have consequences on the properties of the material. The results explain recent magnetic measurements from such samples.

4.3.2 Paper IX: Defect structure of $Ga_{1-x}Mn_xAs$: A cross-sectional scanning tunneling microscopy (XSTM) study

In this paper a study of $Ga_{1-x}Mn_xAs$ with Mn concentrations of 0.7%, 2%, 5%, and 7% is presented. Bright protrusions close to the top layer As atoms in the GaAs (110) could be correlated to the Mn concentration in the samples. Atomically resolved filled and empty states

XSTM images of this defect are compared to first principle simulations of the STM images with the Mn atoms in different sites in the GaAs lattice. By combining the experimental and theoretical results, it is concluded that the Mn related protrusions result from substitutional Mn in the second layer Ga site. The results demonstrate that the Mn atoms appear as protrusions in both filled and empty state images, and provide an interpretation of XSTM images of $Ga_{1-x}Mn_xAs$ compounds. Further, the presence of any substitutional Mn in the top-most Ga layer is excluded, demonstrating that a rearrangement of the $Ga_{1-x}Mn_xAs$ surface occurs immediately after cleavage. The study shows that significant deviations from the expected bulk terminated surface occur when cleaving GaMnAs, resulting in a nontrivial interpretation of the STM images displaying atomic resolution.

Bibliography

[1] R. M. Feenstra, Semicond. Sci. Technol. **9**, 2157 (1994).

[2] Ph. Ebert, Surf. Sci. Rep. **33**, 121 (1999).

[3] R. S. Goldman, J. Phys. D: Appl. Phys **37**, 163 (2004).

[4] A. Mikkelsen and E. Lundgren, Prog. Surf. Sci. **80**, 1-25 (2005).

[5] S. M. Sze, *Semiconductor Devices, Physics and Technology* (John Wiley & Sons, New York, 2002, 2nd edition).

[6] Charles Kittel, *Introduction to Solid States Physics* (John Wiley & Sons, New York, 1986, sixth edition).

[7] J. C. Phillips, *Bonds and Bands in Semiconductors* (Academic Press, 1973).

[8] A. H. MacDonald, P. Schiffer and N. Samarth, Nature Materials **4**, 195 (2005).

[9] J. A. Gaj, J. Ginter and R. R. Galazka, Phys. Status Solidi (b) **89**, 655 (1978).

[10] M. Jaczynski, J. Kossut and R. R. Galazka, Phys. Status Solidi (b) **88**, 73 (1978).

[11] T. Jungwirth, J. Sinova, J. Masek, J. Kucera and A. H. MacDonald, Preprint: cond-mat/0603380, Rev. Mod. Phys. in press.

[12] H. Ohno, A. Shen, F. Matsukura, T. Omiya, A Endo, S. Katsumoto and Y. Iye, Appl. Phys. Lett. **69**, 363 (1996).

[13] T. Dietl, H. Ohno, F. Matsukura, J. Cibert and D. Ferrand, Science **287**, 1019 (2000).

[14] R. Shioda, K. Ando, T. Hayashi and M. Tanaka, Phys. Rev. B **58**, 1100 (1998).

[15] S. J. Potashnik, K. C. Ku, S. H. Chun, J. J. Berry, N. Samarth and P. Schiffer, Appl. Phys. Lett. **79**, 1495 (2001).

[16] H. Ohno, Mat. Sci. Eng. B **84**, 70 (2001).

[17] M. Bayer and A. Forchel, Phys. Rev. B **615**, 041308R (2002).

[18] J. N. Randall, M. A. Reed, R. J. Matyi and T. M. Moore, J. Vac. Sci. Technol. B **6**, 1861 (1988).

[19] M. A. Reed, J. N. Randall, R. J. Aggarwal, R. J. Matyi, T. M. Moore and A. E. Wetsel, Phys. Rev. Lett. **60**, 535 (1988).

[20] M. Borgström, T. Bryllert, B. Gustafson, J. Johansson, T. Sass, L. E. Wernersson, W. Seifert and L. Samuelsson, J. Electron. Mater. **30**, 482 (2001).

[21] T. Bryllert, M. Borgström, L. E. Wernersson, W. Seifert and L. Samuelsson, Appl. Phys. Lett. **82**, 2655 (2003).

[22] T. Bryllert, M. Borgström, T. Sass, B. Gustafson, L. Landin, L. E. Wernersson, W. Seifert and L. Samuelsson, Appl. Phys. Lett. **80**, 2681 (2002).

[23] D. Bimberg, M. Grundmann and N.N. Ledentsov, *Quantum Dot Heterostructures* (John Wiley & Sons, Chichester, 1999).

[24] L. Landin, M. Borgström, M. Kleverman, M. -E. Pistol, L. Samuelson, W. Seifert and X. H. Zhang, Thin Solid Films **364**, 161 (2000).

[25] S. Hinooda, S. Frechengues, B. Lambert, S. Loualiche, M. Paillard, X. Marie and T. Amand, Appl. Phys. Lett. **75**, 3530 (1999).

[26] Y. M. Manz, O. G. Schmidt and K. Eberl, Appl. Phys. Lett. **76**, 3343 (2000).

[27] Zia, *Quantum Dot Solutions*, http://www.zialaser.com

[28] A. Zrenner, E. Beham, S. Stufler, F. Findeis, M. Bichler and G. Abstreiter, Nature **418**, 612 (2002).

[29] Z. Yuan, B. E. Kardynal, R. M. Stevenson, A. J. Shields, C. J. Lodo, K. Cooper, N. S. Beattie, D. A. Ritchie and M. Pepper, Science **295**, 102 (2002).

[30] C. Santori, D. Fattal, J. Vuckovic, G. S. Solomon and Y. Yamamoto, Nature **419**, 594 (2002).

[31] T. Lundström, W. Schoenfeld, H. Lee and P. M. Petroff, Science **286**, 2312 (1999).

[32] L. Goldstein, F. Glas, J. Y. Marzin, M. N. Charasse and G. L. Roux, Appl. Phys. Lett. **47**, 1099 (1985).

[33] Q. Xie, A. Madhukar, P. Chen and N. P. Kobayashi, Phys. Rev. Lett. **75**, 2542 (1995).

[34] L. L. Chang, L. Esaki and R. Tsu, Appl. Phys. Lett. **24**, 593 (1974).

[35] S. Raghavan, P. Rotella, A. Stintz, B. Fuchs, S. Krishna, C. Morath, D. A. Cardimona and S. W. Kennerly, Appl. Phys. Lett. **81**, 1369 (2002).

[36] E. T. Kim, A. Madhukar, Z. Ye and J. C. Campbell, Appl. Phys. Lett. **84**, 3277 (2004).

[37] Sanjay Krishna, J. Phys. D: Appl. Phys. **38**, 2142 (2005).

[38] S. Raghavan, D. Forman, P. Hill, N. R. Weisse-Bernstein, G. von Winckel, P. Rotella, S. Krishna, S. W. Kennerly and J. W. Little, J Appl. Phys. **96**, 1036 (2004).

[39] E. T. Kim, Z. Chen and A. Madhukar, Appl. Phys. Lett. **81**, 3473 (2002).

[40] S. Krishna, S. Raghavan, G. von Winckel, P. Rotella, A. Stintz, C. P. Morath, D. Le and S. W. Kennerly, Appl. Phys. Lett. **82**, 2574 (2003).

[41] E. T. Kim, Z. Chen and A. Madhukar, Appl. Phys. Lett. **79**, 3341 (2001).

[42] R. S. Wagner, in: A. P. levit (Ed), Whisker Techn. (Wiley-Interscience, New York, 1970) pp 47-119.

[43] K. Hiruma, M. Yazawa, T. Katsuyama, K. Ogawa, K. Haraguchi, M. Koguchi and H. Kakibayashi, J. Appl. Phys. **77**, 447 (1995).

[44] G. Zheng, F. Patolsky, Y. Cui, W. U. Wang, and C. M. Lieber, Nature Biotechnology **23**, 1294 (2005).

[45] L. Samuelson, Materials Today **6**, 22 (2003).

[46] J. Goldberger, A. I. Hochbaum, R. Fan and P. Yang, Nano Lett. **6**, 973 (2006).

[47] J. Wang, M. S. Gudiksen, X. Duan, Y. Cui and C. M. Lieber, Science **293**, 1455 (2001).

[48] C. Thelander, H. A. Nilsson, L. E. Jensen and L. Samuelson, Nano Lett. **5**, 635 (2005).

[49] J. B. Hannon, S. Kodambaka, F. M. Ross and R. M. Tromp, Nature 04574 (2006).

[50] T. Bryllert, L. E. Wernersson, L. Jensen and L. Samuelson IEEE Electron Device Lett. **5**, 323 (2006).

[51] Y. Cui, Q. Wei, H. Park and C. M. Lieber, Science **293**, 1289 (2001).

[52] F. C. Frank and J. H. V. d. Merwe, Proc. R. Soc. London Ser. A **198**, 205 (1949).

[53] M. Volmer and A. Weber, Z. Physik. Chem. **119**, 277 (1926).

[54] I. N. Stanski and L. Krastanow, Sitz. Ber. Akad. Wiss., Math. -Naturwiss. K1. Abt. IIb **146**, 797 (1938).

[55] R. S. Wagner and W. C. Ellis, Appl. Phys. Lett. **4**, 89 (1964).

[56] T. I. Kamins, R. S. Williams, D. P. Basile, T. Hesjedal and J. S. Harris, J. Appl. Phys. **89**, 1008 (2001).

[57] H. Y. Tuan, D. C. Lee, T. Hanrath and B. A. Korgel, Nano Lett. **5**, 681 (2005).

[58] A. I. Persson, M. W. Larsson, S. Stenström, B. J. Ohlsson, L. Samuelson and L. R. Wallenberg, Nature Materials **3**, 677 (2004).

[59] Roland Wisendanger, *Scanning Probe Microscopy and Spectroscopy, Methods and Applications* (Cambridge University Press 1994).

[60] L. J. Whitman, Naval Research Laboratory, Whashington, DC 20375-5342, *The Encyclopedia of Applied Physics* (VCH).

[61] A. Mikkelsen, L. Ouattara and E. Lundgren, Surf. Sci. **557**, 109 (2004).

[62] Dawn A. Bonnell, *Scanning Tunneling Microscopy and Spectroscopy, Theory, Techniques and Applications* (VCH Publishers, Inc., New York, 1993).

[63] J. Tersoff and D. R. Hamann, Phys. Rev. Lett. **50**, 1998 (1983).

[64] J. Tersoff and D. R. Hamann, Phys. Rev. B **31**, 805 (1985).

[65] J. Bardeen, Phys. Rev. Lett. **6**, 57 (1961).

[66] R. M. Feenstra, J. A. Stroscio, J. Tersoff and A. P. Fein, Phys. Rev. Lett. **58**, 1192 (1987).

[67] A. Hofer, S. Foster and L. Shluger, Rev. Mod. Phys. **75**, 1287 (2003).

[68] G. Cross, A. Schirmeisen, A. Stalder, P. Grutter and U. Dürig, Phys. Rev. Lett. **80**, 4685 (1998).

[69] R. M. Feenstra and A. P. Fein, Phys. Rev. B. **32**, 1192 (1985).

[70] B. Legrand, B. Grandidier, J. P. Nys, D. Stiévenard, J. M. Gerard and V. Thierry-Mieg, Appl. Phys. Lett. **73**, 96 (1998).

[71] H. Eisele, O. Flebbe, T. Kalka, C. Preinesberger, F. Heinrichsdorff, A. Krost, D. Bimberg and M. Dhäne- Priestsch, Appl. Phys. Lett. **75** 106 (1999).

[72] D. M. Bruls, J. W. A. M. Vugs, P. M. Koenraad, H. W. M. Salemink and J. H. Wolter, Appl. Phys. Lett. **81** 1708 (2002).

[73] Henrik Davidsson, *Cross-sectional scanning tunneling microscopy studies of GaMnAs superlattices*, M. Sc. thesis, Lund University, 2004.

[74] A. Mikkelsen, L. Ouattara, H. Davidsson, E. Lundgren, O. Pacherova and J. Sadowski, Appl. Phys. Lett. **85**, 4660 (2004).

[75] A. Mikkelsen, B. Sanyal, J. Sadowski, L. Ouattara, J. Kanski, S. Mirbt, O. Eriksson and E. Lundgren, Phys. Rev. B **70**, 085411 (2004).

[76] D. M. Bruls, J. W. A. M. Vugs, P. M. Koenraad, H. W. M. Salemink and J. H. Wolter, Appl. Phys. Lett. **81**, 1708 (2002).

[77] D. M. Bruls, P. M. Koenraad, H. W. M. Salemink, J. H. Wolter, M. Hopkinson and M. S. Skolnick, Appl. Lett. **82**, 3758 (2003).

[78] A. Lorke, R. J. Luyken, A. O. Govorov, J. P. Kotthauss, J. M. Garcia and P. M. Petroff, Phys. Rev. Lett. **84**, 2223 (2000).

[79] H. Sugiura, T. Nishida, R. Iga, T. Yamada and T. Tamamura, J. Cryst. Growth **121**, 579 (1992).

[80] K. Park, H. Hwang, J. -H. Kang, S. Yoon, Y. D. Kim and E. Yoon, J. Cryst. Growth **248**, 201 (2003).